HIF1A contributes to the survival of aneuploid and mosaic pre-implantation embryos

Estefania Sanchez-Vasquez[1], Marianne E. Bronner[1] and Magdalena Zernicka-Goetz[1,2*]

[1]Division of Biology 139-74, California Institute of Technology, Pasadena, CA 91125, USA.
[2]Department of Physiology, Development and Neuroscience, University of Cambridge, Cambridge, UK.
*Lead and correspondence: magdaz@caltech.edu

Running title
HIF1A role in aneuploid and mosaic embryos

Key words
Embryogenesis/ Aneuploidy/ Mosaic embryos/ DNA repair/ Hypoxia

ABSTRACT

Human fertility is suboptimal, partly due to error-prone divisions in early cleavage-stages that result in aneuploidy. Most human pre-implantation are mosaics of euploid and aneuploid cells, however, mosaic embryos with a low proportion of aneuploid cells have a similar likelihood of developing to term as fully euploid embryos. How embryos manage aneuploidy during development is poorly understood. This knowledge is crucial for improving fertility treatments and reducing developmental defects. To explore these mechanisms, we established a new mouse model of chromosome mosaicism to study the fate of aneuploid cells during pre-implantation development. We previously used the Mps1 inhibitor reversine to generate aneuploidy in embryos. Here, we found that treatment with the more specific Mps1 inhibitor AZ3146 induced chromosome segregation defects in pre-implantation embryos, similar to reversine. However, AZ3146-treated embryos showed a higher developmental potential than reversine-treated embryos. Unlike reversine-treated embryos, AZ3146-treated embryos exhibited transient upregulation of Hypoxia Inducible-Factor-1A (HIF1A) and lacked p53 upregulation. Pre-implantation embryos develop in a hypoxic environment *in vivo*, and hypoxia exposure *in vitro* reduced DNA damage in response to Mps1 inhibition and increased the proportion of euploid cells in the mosaic epiblast. Inhibiting HIF1A in mosaic embryos also decreased the proportion of aneuploid cells in mosaic embryos. Our work illuminates potential strategies to improve the developmental potential of mosaic embryos.

INTRODUCTION

Humans exhibit suboptimal fertility relative to other mammals (Palmerola et al., 2022a). Only ~30% of human conceptions progress to live birth (Capalbo et al., 2021). Intriguingly, the first zygotic cleavage-stage divisions in human embryos are error prone, generally resulting in aneuploidy, in which cells gain or lose chromosomes (Allais & FitzHarris, 2022; Currie et al., 2022; Palmerola et al., 2022b; Pauerova et al., 2020; Vanneste et al., 2009). A high incidence of aneuploidy in the early cleavage divisions is thought to underlie low human fecundity and most developmental defects (Palmerola et al., 2022a). Both *in vivo* and *in vitro* fertilization (IVF) often give rise to mosaic embryos of diploid and aneuploid cells. Although it is predicted

that ~60% of pre-implantation IVF embryos exhibit diploid-aneuploid mosaicism (Capalbo et al., 2021), our understanding of the embryo's ability to cope with such abnormalities is limited.

The incidence of aneuploidy declines at later stages of development (Shahbazi et al., 2020), but the mechanism underlying this decline is poorly understood. Human mosaic embryos can develop to term (Capalbo et al., 2021; Greco et al., 2015; Starostik et al., 2020). Specifically, implantation of low- and medium-grade mosaic embryos, defined as having 20-30% and 30-50% aneuploid extra-embryonic trophectoderm cells in a biopsy, has been reported to be as likely to result in the birth of healthy babies as implantation of fully euploid embryos (Capalbo et al., 2021). Given that some mosaic embryos are able to develop to term, it is important to uncover the mechanisms that confer their viability.

Mouse models of chromosome mosaicism enable analyses that are not allowed with human embryos for ethical reasons. Mouse and human pre-implantation development are very similar to each other: both undertake cleavage divisions, compaction, blastocyst cavity formation and hatching, albeit with slightly different timings in the two species (Mole et al., 2020; Zhu et al., 2021). During pre-implantation development, cells on the outside of the embryo form the extra-embryonic trophectoderm (TE) whereas cells on the inside form the pluripotent inner cell mass (ICM). Subsequently, cells of the ICM are segregated into the embryonic epiblast (EPI) and extra-embryonic primitive endoderm (PE). The TE will form the placenta, the PE will form the yolk sac and the EPI will form the fetus (Zhu & Zernicka-Goetz, 2020) .

Recently, our group developed the first mouse model of chromosome mosaicism, based on the generation of aneuploidies induced by a drug reversine (Bolton et al., 2016; Singla et al., 2020). Reversine is a pan-Aurora kinase inhibitor that also antagonizes the A3 adenosine receptor and inhibits mitotic kinase monopolar spindle 1 (MPS1) (D'Alise et al., 2008; Santaguida et al., 2010). Our analysis revealed that reversine-treated mosaic embryos are aneuploid and overexpress p53 (Bolton et al., 2016). Importantly, reversine-treated cells in mosaic embryos are gradually eliminated from the EPI, particularly around the time of blastocyst implantation. As with human mosaic embryos (Capalbo et al., 2021), we found that murine mosaic embryos with at least 50% of euploid cells had a similar developmental potential as fully euploid embryos (Bolton et al., 2016; Singla et al., 2020).

As reversine affects p53 and may compromise cellular fitness (D'Alise et al., 2008; Santaguida et al., 2010), we sought to generate a complementary aneuploid model. To this end, we used the more specific Mps1 inhibitor, AZ3146 (Hewitt et al., 2010). Although AZ3146 and reversine both interfere with the spindle assembly checkpoint (Hewitt et al., 2010), they bind to Mps1 in a different manner (Lan & Cleveland, 2010). In mouse embryos, AZ3146 treatment was shown to double the occurrence of micronuclei, a marker of chromosome segregation defects, but without negatively affecting cellular fitness (Vazquez-Diez et al.,

2019). In the present study, we used AZ3146- and reversine-treated pre-implantation mouse embryos to dissect the mechanisms underlying aneuploid cell elimination and survival.

RESULTS

AZ3146 treatment induces chromosome segregation defects in pre-implantation mouse embryos.

To generate distinct models of aneuploidy, we treated 4- to 8-cell stage mouse embryos with AZ3146 (20 μM) (Vazquez-Diez et al., 2019), as well as with reversine (0.5 μM) (Bolton et al., 2016) as a positive control, or DMSO (vehicle) as a negative control (Fig. 1A). We evaluated how the different Mps1 inhibitors affect chromosome segregation by detecting nuclei and kinetochores in 8-cell embryos and counted chromosomes *in situ* (Pauerova et al., 2020). Micronuclei were identified as small DAPI-stained chromosomes that were clearly distinct from the nuclei (Fig. S1A). We examined 32 DMSO-treated control embryos and observed only 22 cells with micronuclei out of a total of 256 cells (Fig. S1B). In contrast, we observed 82 cells with micronuclei in a total of 144 individual cells from 18 reversine-treated embryos, and 182 cells in a total of 304 individual cells from 38 AZ3146-treated embryos (Fig. S1A). After normalization, the average of aneuploidy in DMSO-treated 8-cell embryos was 12.5%, compared to 75% in the reversine-treated embryos and 62.5% in the AZ3146-treated embryos (Fig. S1B). We also detected non-dividing nuclei as rounded circles with distinct DAPI intensities in embryos treated with reversine and AZ3146. Specifically, we observed 28 non-dividing cells (19%) in reversine-treated embryos and 24 non-dividing cells (7.9%) in AZ3146-treated blastomeres, but none in DMSO-treated blastomeres (Fig. S1B). The increased frequencies of micronuclei and non-dividing cells in response to Mps1 inhibition are consistent with elevated aneuploidy and chromosomal instability (Daughtry and Chavez, 2016; Vazquez-Diez et al., 2016), as we showed previously for reversine-treated embryos (Bolton et al., 2016).

Given these distinct responses to reversine and AZ3146, we examined how these treatments impact the lineages in the blastocyst. To this end, we treated embryos with DMSO, reversine or AZ3146 from the 4- to 8-cell stage, and then washed and cultured them until the late blastocyst stage (E4.5). We assessed lineages by immunofluorescence (IF) to detect the TE marker CDX2, the EPI marker NANOG, and the PE marker SOX17. We found that all lineages segregated normally, and that blastocyst morphology was similar in all three conditions (Fig. 1B). We quantified the number of cells in the blastocysts and found that DMSO-treated controls had a median of 93 cells in total, whereas reversine- and AZ3146-treated embryos had a median of only 79 and 82 cells, respectively (***$P<0.0004$, *$P<0.05$, Mann–Whitney U-test, n=28 embryos per treatment collected from three independent experiments) (Fig. 1C). DMSO-treated blastocysts contained a median of 15 EPI, 11 PE, and 67 TE cells, whereas reversine-treated blastocysts contained 12 EPI, 8 PE and 59 TE cells, and AZ3146-treated blastocysts had 11 EPI, 7 PE and 64 TE cells (Fig. 1C). These data suggest that reversine treatment compromises the development of all three lineages, as observed previously (Bolton et al., 2016), whereas AZ3146 mainly compromises ICM (EPI and PE) development.

To compare the developmental potential of blastocysts that had been treated with AZ3146 or reversine, we transferred them into opposite uterine horns of the same mouse and counted decidua, which reflect successful implantation, as well as viable embryos at E9.5. Although two (8%) reversine-treated blastocysts developed decidua (Fig. S1C), none gave rise to viable E9.5 embryos. In contrast, seven (30%) AZ3146-treated blastocysts developed decidua and five (21%) generated viable E9.5 embryos (Fig. S1D). Thus, AZ3146-treated embryos appear to have a higher developmental potential than reversine-treated embryos.

Considering that cellular fitness and aneuploid stress are related to DNA damage and DNA repair, we first sought to understand if these parameters were affected in our drug treatments. We used IF to quantify the levels of the DNA repair marker PARP1 and of the DNA damage marker, phosphorylated H2A.X (γH2A.X) at the 8-cell and morula stages (Fig. 1D). We observed elevated γH2A.X levels in reversine- and AZ3146-treated 8-cell embryos compared to controls (Fig. 1E), which eventually returned to normal in AZ3146-treated blastocysts, but not in reversine-treated blastocysts (Fig. S2A).

PARP1 was specifically enriched in the EPI lineage in normal blastocysts, as assessed by IF and re-analysis of published scRNA-seq data (Deng et al., 2014) (Fig. S2B). Intriguingly, PARP1 levels were reduced at the 8-cell and morula stages in reversine-treated embryos compared to controls and to AZ3146-treated embryos (Fig. 1 D-E). Moreover, late morula stage embryos treated with the PARP inhibitor Olaparib (10 μM, Hou et al., 2022; Prasad et al., 2017) developed into smaller blastocysts with only 78 total cells, reflecting a relatively low number of ICM cells, only 8 EPI and 4 PE cells in DMSO-treated embryos (Fig. S2C-E). Treatment with reversine, but not AZ3146, further reduced the number of cells in the EPI lineage of Olaparib-treated embryos (Fig. S2E). Overall, these data suggest that PARP1 is required for proper development of the ICM, and that its reduced levels after reversine treatment may negatively impact development.

Reversine and AZ3146 activate distinct stress response pathways in pre-implantation embryos.

Chromosome mis-segregation and aneuploidy are associated with different cellular stress pathways (Zhu et al., 2018). For instance, p53 is frequently activated following DNA damage, which can limit proliferation and trigger apoptosis (Abuetabh et al., 2022; Soto et al., 2017; Thompson & Compton, 2010). The p38 mitogen-activated protein kinase (MAPK) can also be activated following DNA damage (Thompson and Compton, 2010). In aneuploid cells, p38 promotes apoptosis by inhibiting the transcription factor Hif-1α (Simoes-Sousa et al., 2018), which otherwise promotes cell survival, proliferation, and metabolic changes in aneuploid cells and in response to hypoxia in different contexts (Hu et al., 2003; Simoes-Sousa et al., 2018).

151 To investigate how treatment with reversine or AZ3146 affect *p53* and *Hif1a* expression in mouse embryos,
152 we performed RT-qPCR at the morula and blastocyst stages. We normalized to *Ppia* (Peptidylprolyl
153 Isomerase A) mRNA, which is a stable reference gene in diploid and polyploid embryos (Gu et al., 2014).
154 Reversine-treated embryos displayed a significant increase in *p53* transcript levels at the morula (7-fold)
155 and blastocyst (1.3-fold) stages compared with DMSO-treated embryos (**P<0.01, *P<0.05, Welch's t-test)
156 (Fig. 2A), as we showed previously (Singla et al., 2020). In addition, reversine-treated embryos showed
157 reduced expression of *Hif1a* at the blastocyst stage, which would be consistent with p38 activation. In
158 contrast, AZ3146-treated embryos did not show upregulation of *p53* at either the morula or blastocyst stage
159 (Fig. 2A). Moreover, AZ3146-treated embryos showed a transient increase in *Hif1a* mRNA levels (3-fold)
160 at the morula stage compared to DMSO- and reversine-treated embryos (Fig. 2A), which returned to normal
161 levels at the blastocyst stage. HIF1A protein was present in DMSO- and reversine-treated embryos and
162 elevated at the morula and blastocyst stages in AZ3146-treated embryos (****P<0.0001, **P<0.01, *P<0.05,
163 Mann–Whitney U-test) (Fig. 2B). HIF1A appeared to be mostly nuclear in morula, but mostly cytoplasmic
164 in blastocysts, under all three conditions (Fig. 2B). Overall, these data suggest that treatment with reversine,
165 but not AZ3146, induces multiple stress pathways in pre-implantation embryos. These differences may
166 contribute to the increased developmental potential of embryos treated with AZ3146 versus reversine.
167
168 **HIF1A activity is required for proper blastocyst formation after Mps1 inhibition.**
169 It was previously shown that Hif1α$^{-/-}$ embryos undergo developmental arrest and lethality by E11 (Iyer et
170 al., 1998). To assess the role of HIF1A in the embryo's response to reversine and AZ3146, we used a
171 pharmacological approach to inhibit its function. Briefly, we tested two different small molecules that have
172 been shown to inhibit HIF1A activity, PX-478 (Lee & Kim, 2011; Zhao et al., 2015) and IDF-11774 (Ban et
173 al., 2017). We treated control zygotes with DMSO, PX-478 (2 μM), or IDF-11774 (20 μM) until the blastocyst
174 stage (Fig. S3A). Unlike PX-478, IDF-11774 treatment did not significantly affect the total number of cells
175 in the TE or the whole blastocyst compared to the control (****P<0.0001, Mann–Whitney U-test) (Fig. S3B).
176 Therefore, we used IDF-11774 to inhibit HIF1A in subsequent experiments.
177
178 Next, we treated embryos with DMSO, reversine, or AZ3146 from the 4- to 8-cell stage, washed them, and
179 then inhibited HIF1A with IDF-11774 from the 8-cell to blastocyst stage (Fig. 2C). Inhibition of HIF1A did
180 not abolish cavitation but dramatically lowered the number of TE and especially PE cells in AZ3146-treated
181 embryos compared to DMSO-treated controls (Fig. 2D) and compared to AZ3146-treated embryos not
182 exposed to IDF-11884 (Fig. 1C). Inhibition of HIF1A also lowered the number of cells in reversine-treated
183 embryos compared to controls, but the effect was smaller (Fig. 2D). Overall, our data suggest that elevated
184 HIF1A activity from the 8-cell stage onwards is particularly important to promote the survival of aneuploid
185 TE and PE cells after AZ3146 treatment.
186

187 Taken together, our data suggest that AZ3146 and reversine have distinct effects on the pre-implantation
188 embryo. Compared to reversine-treated embryos, AZ3146-treated embryos appear to have increased
189 developmental potential, lack upregulation of p53, and show transient upregulation of *Hif1a*. Moreover,
190 AZ3146-treated embryos have a greater dependence on HIF1A activity to form the TE and PE.
191
192 **Hypoxia exposure attenuates DNA damage and blastomere defects in response to Mps1 inhibition.**
193 Pre-implantation development occurs in a hypoxic environment, and many clinics culture human embryos
194 under hypoxic conditions (5%) (Houghton, 2021). It was reported that physiologic oxygen concentrations
195 can improve the yield and quality of mammalian blastocysts (Ciray et al., 2009; Nguyen et al., 2020) and
196 increase the nuclear translocation of HIF1A in mouse blastocysts (Choi et al., 2021) To investigate how
197 hypoxia affects the development of euploid and aneuploid mouse embryos, we repeated our experiments
198 performed under normoxia (air, 20% O_2/5% CO_2; control) (Fig. 1A) in hypoxic (5% O_2/5% CO_2) conditions
199 (Fig. 3A). We cultured embryos from the 2-cell stage until the blastocyst stage, treating them with DMSO,
200 reversine, or AZ3146 from the 4-8 cell stage.
201
202 First, we examined lineage specification by quantifying the cell numbers in all three lineages at the
203 blastocyst stage. We found that DMSO-treated blastocysts cultured under hypoxia had a median of 74
204 cells, representing 14 EPI cells, 6 PE cells and 54 TE cells (Fig. 3B-C). These data suggest that, under our
205 conditions, the cell number in the pre-implantation mouse blastocyst is reduced when cultured in hypoxia
206 compared to normoxia (Fig. 3C, 1C), particularly in the TE and PE. Notably, reversine and AZ3146
207 treatment did not further reduce cell numbers for embryos cultured under hypoxia, except for in the PE (Fig.
208 3C).
209
210 To investigate how hypoxia exposure affects DNA damage and repair in mouse embryos, we again
211 performed IF for γH2A.X and PARP1 in 8-cell embryos and morula. We found that hypoxia exposure
212 lowered the levels of γH2A.X under all conditions, and minimized the differences between DMSO, reversine
213 and AZ3146 treatments. In addition, PARP1 levels were also similar under all conditions, and relatively low
214 in morula (Fig. 3D-E). Overall, these data suggest that hypoxia exposure lowers the accumulation of DNA
215 damage under all conditions.
216
217 **Hypoxia increases the proportion of euploid cells in the epiblast of mosaic blastocysts.**
218 Despite the high incidence of mosaicism in human pre-implantation embryos, the fate of aneuploid cells in
219 mosaic embryos is incompletely understood. We previously used reversine to generate a mouse model of
220 pre-implantation chromosome mosaicism and found that aneuploid (Reversine-treated) cells are eliminated
221 in the EPI of mosaic embryos via apoptosis, starting from the mature blastocyst stage (Bolton et al., 2016).
222 Whether this response reflects reversine treatment specifically, or aneuploidy more generally, is not known.
223 Moreover, how hypoxia versus normoxia affects the outcomes is also not clear.

224

225 To address these questions, we created aggregation chimeras at the 8-cell stage that contained a 1:1 ratio
226 of AZ3146-treated and control blastomeres (DMSO/AZ3146 chimeras), which is expected to reflect low-
227 grade mosaicism, or of AZ3146-treated and reversine-treated blastomeres (reversine/AZ3146 chimeras),
228 which is expected to reflect medium-grade mosaicism (Fig. 4A). We cultured these chimeric embryos in
229 normoxia and hypoxia, and followed the fate of individual blastomeres by using transgenic mouse lines with
230 the membrane markers mTmG (Muzumdar et al., 2007) and E-cadherin (Christodoulou et al., 2019).
231 DMSO/AZ3146 and reversine/AZ3146 blastocysts displayed proper lineage allocation, embryo morphology
232 and cavitation in both normoxia and hypoxia (Fig. 4B-C). In addition, DMSO/AZ3146 and reversine/AZ3146
233 embryos had comparable total cell numbers in their blastocysts, and blastocysts grown in hypoxia were
234 again smaller than those grown in normoxia (Fig. 4D-E). Intriguingly, despite having fewer total cells,
235 DMSO/AZ3146 blastocysts had more EPI cells when they were cultured in hypoxia compared to normoxia
236 (Fig. 4D-E).
237

238 We quantified the proportion of AZ3146 cells in each lineage for each chimera. In DMSO/AZ3146-treated
239 blastocysts, we found that 46.75% of the TE and 42.88% of the EPI originated from AZ3146-treated
240 blastomeres, compared to only 28.57% of the PE (Fig. 4F). In reversine/AZ3146 chimeras, 63% of the TE
241 and 78.4% of the EPI originated from AZ3146-treated cells, compared to only 40% of the PE (Fig. 4F).
242 Thus, under normoxia, DMSO cells appear to outcompete AZ3146-treated cells, which in turn outcompete
243 Reversine-treated cells in the TE and EPI. AZ3146-treated cells appeared to be at a competitive
244 disadvantage in the PE in both contexts. Culturing DMSO/AZ3146 chimeras in hypoxia considerable
245 increased the representation of AZ3146-treated blastomeres in the TE (49.06%) and PE (50%) but,
246 strikingly, reduced their representation in the EPI (33.3%) (Fig. 4G). These altered frequencies reflect a
247 higher number of DMSO-treated cells in the EPI and a lower number in the PE (Fig. 4E). Hypoxia exposure
248 of reversine/AZ3146 embryos lowered the contribution of AZ3146-treated blastomeres to the TE (55.94%)
249 and EPI (50%) but not the PE (46.43%) (Fig. 4G). We found that there was no correlation between the
250 proportion of AZ3146-treated cells in the TE and the EPI in DMSO/AZ3146 and reversine/AZ3146 chimeras,
251 under hypoxia or normoxia, and that hypoxia seemed to have a greater impact on the proportion of AZ3146
252 cells in reversine/AZ3146 chimeras (Fig. S4). Overall, these data suggest that hypoxia has lineage-specific
253 effects on competitions between aneuploid and euploid cells and increases the contribution of euploid cells
254 to the EPI.
255

256 Blastomeres in the 4-cell stage embryo display a lineage bias (Goolam et al., 2016). We considered that
257 mosaicism generated before the 4-cell stage might influence lineage allocation. To test this possibility, we
258 treated zygotes with reversine or AZ3146 during the first cleavage division. Importantly, reversine treatment
259 at the zygote stage seems to strongly affect the morphology of the blastocysts (Fig. S5A). Consistent with
260 this change in morphology, reversine-treatment reduced the number of cells in all lineages, particularly in

261 the TE and PE (Fig. S5B). In contrast, AZ3146 treatment did not affect morphology or cell number in any
262 of the lineages (Fig. S5A-B) (n>27 embryos per treatment, cumulative of three independent experiments,
263 ****P<0.0001, *P<0.0044, Mann–Whitney U-test). To evaluate how early generation of aneuploidies in the
264 embryos affect cell competition, we generated DMSO/AZ3146, Reversine/DMSO, and Reversine/AZ3146/
265 aggregation chimeras at the 2-cell stage and cultured them under normoxia until the blastocyst stage (Fig.
266 S5C). We found that all three 2-cell stage aggregation chimeras developed into blastocysts with proper
267 lineage segregation and the presence of a cavity (Fig. S5D). Interestingly, the reversine-treated cells were
268 extruded from the blastocyst in 54% of the reversine/DMSO chimeras and in 33% of the AZ3146/reversine
269 chimeras, whereas no cell extrusion was observed in the DMSO/AZ3146 chimeras. Quantification of the
270 proportion of AZ3146-treated cells in 2-cell stage derived chimeras (Fig. S5E) showed similar results as 8-
271 cell stage derived chimeras (Fig. 4F-G). In DMSO/AZ3146-treated blastocysts, we found that 49.28% of
272 the TE, 39% of the EPI and 33.33% of the PE originated from AZ3146-treated blastomeres (Fig. S5E). In
273 reversine/AZ3146 chimeras, 68.24% of the TE, 68.83% of the EPI, and 66.67% of the PE originated from
274 AZ3146-treated cells (Fig. S5E). In DMSO/reversine chimeras, 22.27% of the TE, 26.98% of the PE, and
275 31.7% of the EPI originated from reversine-treated cells. Overall, these results suggest that aneuploidy
276 generated at different stages similarly affect the proportion of aneuploid cells in the blastocysts.
277
278 **HIF1A inhibition reduces the frequency of aneuploid cells in DMSO/AZ3146 mosaic embryos.**
279 Our data suggest that hypoxia affects aneuploid-euploid cell competition in mosaic embryos (Fig. 4). To
280 further assess the effect of HIF1A and, considering most human embryos are culture under hypoxic
281 conditions, we decided to evaluate the effect of inhibiting HIF1A in mosaic embryos cultured in hypoxic
282 conditions. We assembled DMSO/AZ3146 and Reversine/AZ3146 8-cell stage chimeras, treated them with
283 the HIF1A inhibitor IDF-11774 (Fig. 5A, S6A-B), and then assessed lineage allocation in blastocysts.
284 Treatment of DMSO/AZ3146 chimeras with IDF11774 does not affect lineage segregation in the blastocyst
285 but reduces the cavity diameter (Fig. 5B-C). Additionally, diminish the contribution of AZ3146-treated cells
286 to the TE, but DMSO-treated cells seem to compensate for this loss in the PE and EPI (Fig. 5D, Fig. S6C).
287 Treating Reversine/AZ3146 chimeras with IDF11774 compromised blastocyst morphology and cavitation
288 (Fig. 5E-F) and considerable increased the number of PE and EPI cells (Fig. 5G), without altering the
289 frequency of AZ3146-treated cells (Fig. S6D). Taken together, our data suggest that HIF1A promotes the
290 survival of AZ3146-treated cells in DMSO/AZ3146 chimeras and suggest that inhibiting HIF1A could
291 increase the proportion of karyotypically normal cells in mosaic embryos.
292
293 **DISCUSSION**
294 Aneuploidy is a common event during pre-implantation development (Allais & FitzHarris, 2022; Currie et
295 al., 2022; Palmerola et al., 2022b). Here, we describe different strategies to generate aneuploidy in the
296 early embryo. Our results suggest that: 1) the Mps1 inhibitor, AZ3146, generates aneuploid embryos with
297 enhanced DNA repair and reduced stress responses when compared to reversine-treated embryos. 2)

298 Lineage specific responses to aneuploidy are present during blastocyst development, as we showed
299 previously (Bolton et al., 2016; Singla et al., 2020). 3) HIF1A contributes to the survival of TE and PE cells
300 in AZ3146-treated embryos whereas PARP1 is particularly required in EPI cells in both reversine and
301 AZ3146-treated embryos. 4) Hypoxia enhances DNA repair and affects aneuploid-euploid cell competition
302 in mosaic embryos.
303
304 Reversine-treated mouse embryos upregulate the mRNA levels of senescent markers p53 and p21 (Singla
305 et al., 2020) and fail to give rise to viable embryos (Bolton et al., 2016). Our results further indicate that
306 reversine downregulates PARP1, as previously observed in glioma (Hirakata et al., 2021). Thus, reversine
307 treatment may compromise embryo development due to a combined increase in DNA damage and
308 decrease in DNA repair. In contrast, embryos treated with AZ3146 do not reduce PARP1 levels and have
309 elevated HIF1A, which appears to improve survival of TE and PE cells and developmental potential.
310
311 DNA repair pathways are enhanced under hypoxic environments in somatic cells (Marti et al., 2021;
312 Nakamura et al., 2022; Pietrzak et al., 2018). Similarly, our data show that aneuploid embryos cultured in
313 hypoxia had lower levels of DNA damage at the morula stage, in agreement with previous studies reporting
314 lower levels of γH2A.X in mouse blastocysts recovered from the uterus and in blastocysts cultured in
315 hypoxia compared to blastocysts cultured in normoxia (Houghton, 2021; Meuter et al., 2014). Interestingly,
316 recent studies suggest that hypoxia favors HIF1A's association with PARP1 in cancer cells, increasing DNA
317 repair (Marti et al., 2021; Nakamura et al., 2022; Pietrzak et al., 2018). In the future, a deeper understanding
318 of the regulation of DNA repair in pre-implantation stages would allow us to understand the molecular
319 response of embryos to aneuploid stress.
320
321 Confined placental mosaicism is commonly observed in human pregnancies, and refers to instances where
322 the placenta is aneuploid but the fetus is euploid (McCoy, 2017). We previously found that aneuploid TE
323 cells have an increased cell cycle length and senescence, whereas aneuploid ICM cells have an increased
324 frequency of apoptosis, in reversine-treated embryos (Singla et al., 2020). Therefore, abnormal but viable
325 TE cells could lead to confined placental mosaicism. Our results further suggest that aneuploid cells
326 contributed mostly to the TE, followed by the EPI, are especially depleted from the PE in AZ3146-treated
327 embryos under normoxia. Intriguingly, under hypoxia aneuploid cells were depleted from the EPI and
328 increase in the PE. Overall, our data suggest that hypoxia may affect cell competition in a lineage-specific
329 manner in the pre-implantation embryo, supporting an increased representation of euploid cells in the EPI
330 relative to the PE and TE.
331
332 Finally, our results confirm that the proportion of aneuploid cells in the EPI and TE do not correlate,
333 consistent with aneuploid survival in the TE but elimination from the ICM. These results are not surprising

334 considering the low aneuploidy concordance rates between TE and ICM in human mosaic aneuploid
335 embryos (30–40%) (Dahdouh & Garcia-Velasco, 2021).
336
337 Since low- and medium- grade mosaic human embryos have similar developmental potential as fully
338 euploid embryos (Capalbo et al., 2021; Greco et al., 2015), understanding the molecular pathways involved
339 in the responses to aneuploidy may have translational implications. Given that the extent and proportion of
340 aneuploid cells in mosaic embryos impact survival (Capalbo et al., 2021), we propose that a reduction in
341 aneuploid cells in the blastocyst will favor a successful pregnancy. Here, we downregulated HIF1A as a
342 strategy for reducing aneuploid cells number and found that treatment with IDF-11774 increased the
343 proportion of euploid cells in mosaic embryos. In sum, our study reveals distinct environmental factors that
344 affect the extent and proportion of aneuploid cells within mosaic embryos.
345
346 **MATERIALS AND METHODS**
347 **Pre-implantation embryo culture**
348 Mice were maintained according to national and international guidelines. Four- to six-week-old B6SJLF1/J
349 female mice were injected with 7.5 IU PMSG followed by 7.5 IU hCG 48 h later, to induce superovulation.
350 The females were then mated with B6CBAF1/J males or were indicated, with E-cadherin GFP or mTmG
351 transgenic males. Pre-implantation mouse embryos were recovered 24 h and 40 h after the hCG injection
352 to obtain zygotes and 2-cell stage embryos, respectively in M2 medium (Sigma, M7167). We incubate the
353 embryos in KSOM until 4-cell stage for the aneuploid treatment, around 53 h post hCG. When recovering
354 zygotes, cumulus cells were removed with 0.3% hyaluronidase (Sigma, H4272) in M2. Embryos then were
355 cultured in regular KSOM (Sigma. MR-106) at 37°C under 5% CO_2/air (Normoxia) or with pre-mixed 5%
356 CO_2/ 5% O_2 balance with nitrogen, biologic atmosphere batch (Airgas #Z03NI9022000033)(Hypoxia).
357 B6SJLF1/J females and B6CBAF1/J males were obtained from JAX laboratories. Females were received
358 at 3-4 weeks of age and were maintained in the CALTECH animal facility, where they were housed with 5
359 same-sex littermates on a 12 h light/12 h dark cycle with food and water *ad libitum*. The temperature in the
360 facility was controlled and maintained at 21 °C. All experimental procedures involving the use of live
361 animals, or their tissues were performed in accordance with the NIH guidelines and approved by the
362 Institutional Animal Care and Use Committee (IACUC) and the Institutional Biosafety Committee at the
363 California Institute of Technology (Caltech, protocol number 1772). Reversine (Sigma, R3904), AZ3146
364 (Sigma, SML1427), PX-478 (Selleckchem, S7612), IDF-11774 (Selleckchem, S8771) and olaparib
365 (Selleckchem, S1060) were dissolved in DMSO (Sigma, D2650) before use to specific concentration. They
366 were respectively used at following final concentrations: 0.5 μM, 20 μM, 2 μM, 20 μM and 10 μM. Control
367 embryos were incubated in the equivalent DMSO concentration. Drugs were dissolved in regular KSOM to
368 the concentration of use. DMSO concentration in media should never pass 0.4%.
369
370 **Immunofluorescence**

371 Embryos were fixed in 4% PFA (Thermo Scientific, AA47340) for 20 min at room temperature (RT).
372 Following by three washes with 0.1% Tween-20 (Sigma, P1379) dissolved in PBS (PBST). The embryos
373 were then permeabilized with 0.3%, Triton X-100 (Sigma, X100) in PBS. Washes were then performed
374 three times in PBST before embryos were transferred to blocking solution (3% BSA in PBS) for at least 3h
375 at RT. Incubation with primary antibodies was performed in blocking solution overnight at 4°C. Next day,
376 washes were performed three times in PBST before incubation with Alexa Fluor secondary antibodies
377 (Thermo Fisher Scientific, 1:500) in blocking solution for 2 h. Washes were performed three times before
378 incubation with DAPI (Thermo Fisher Scientific) for 5 min. Washes after DAPI were perform two times in
379 PBST before the final incubation in M2. Embryos were then mounted in M2 micro-drops on 35 mm glass
380 bottom dish (MATTEK, P35G-1.5-14-C). Confocal imaging was carried out using Leica SP8, 40x objective,
381 1 µM Z-step. Image files were viewed and analyzed using ImageJ and IMARIS 9.9 software.
382 Primary antibodies used: mouse anti-CDX2 (Biogenex, 1:500), rabbit anti-NANOG (1:500; Abcam), goat
383 anti-SOX17 (1:300; R&D Systems), rabbit anti-HIF1A (1:300, Novusbio), mouse anti-PARP1 (1:500,
384 Proteintech) and rabbit anti- Phospho- Histone H2AX (1:500, R&D Systems).
385
386 ***In situ* chromosome counting**
387 For determination of aneuploidy, treated 8-cell stage embryos were synchronized in metaphase by 10h
388 treatment with 0.03 µg/mL colcemid (Cayman, 15364) diluted in KSOM. Following by 1h treatment with 10
389 µM Mg132 (Selleckchem, S2619) in KSOM. Finally, 1 h treatment with 5 µM dimethylenastron
390 (MedChemExpress, HY-19944) and 10 µM Mg132 in KSOM. Synchronized embryos were then fix in 2%
391 PFA for 20 min, permeabilized with PBST for 15 min and blocked 3h at RT before incubation with human
392 anti-centromere protein antibody (1:300, Antibodiesinc 15-234) overnight at 4°C. Next day, three washes
393 with PBST were performed before 2 h incubation with goat anti-Human secondary antibody, Alexa Fluor
394 647 (1:400, Invitrogen A-21445) in blocking solution. Washes were performed three times before 20 min
395 incubation with DAPI (1:500) and Alexa Fluor 488 Phalloidin (1:300, Invitrogen A12379). Washes then were
396 performed three times before clearing overnight with AF1 plus (Citifluor, AF1/DAPI-15). Embryos were then
397 mounted in AF1 plus micro-drops on 35 mm glass bottom. Confocal imaging was carried out using Leica
398 SP8, 60x objective, 0.5 µM Z-step. Image files were viewed and analyzed using ImageJ and IMARIS 9.9
399 software.
400
401 **Embryo transfers and post implantation recovery and biopsy**
402 Embryo transfer were performed as described previously (Bermejo-Alvarez et al., 2014). CD1 females and
403 vasectomizes CD1 males were obtained from Charles River. Reversine and AZ3146-treated blastocyst
404 were transfer into 2.5-days pseudopregnant CD1 females. Around 16 AZ3146-treated embryos were
405 transfer in the right uterine horn, whereas around 16 reversine-treated embryos were transfer in the left
406 uterine horn of the same female as control. To evaluate implantation and embryo survival potency, uterine
407 horns were recovered 5 days after surgery. Deciduas were dissected and post implantation embryos at

408 stage E9.5 were recovered into PBST on ice. Embryos were fixed in 4% PFA at RT for 1 h, followed by
409 washes through PBST before imaging. Images were taken using an Olympus LS stereo microscope with a
410 10x objective. Uterine transfers were performed in accordance with the NIH guidelines and approved by
411 the Institutional Animal Care and Use Committee (IACUC) and the Institutional Biosafety Committee at the
412 California Institute of Technology (CALTECH).
413
414 **qRT-PCR**
415 Around 14 to 17 morulas and blastocysts were collected for quantitative reverse transcriptase polymerase
416 chain reaction (qRT-PCR). Total RNA from morulas was obtained using the NucleoSpin RNA Plus XS kit
417 (Takara, 740990.10). Whereas total RNA from blastocyst was extracted using the Arcturus PicoPure RNA
418 Isolation Kit (Thermo Fisher, KIT0204). qRT-PCR was performed using the *Power* SYBR Green RNA-to-
419 CT 1-Step Kit (Applied Biosystems, 4389986) in a StepOne Plus Real-time PCR machine (Applied
420 Biosystems). The following program was used: 30 min 48 °C (reverse-transcription) followed by 10 min 95
421 °C followed by 45 cycles of 15 s 95 °C (denaturing) and 1 min 60 °C (annealing and extension). The ddCT
422 method was used to determine relative levels of mRNA expression, with Ppia as an endogenous control
423 (Gu et al., 2014). Primers were obtained from IDT.

Name	Sequence
p53_Fw	GTCACAGCACATGACGGAGG
p53_Rv	TCTTCCAGATGCTCGGGATAC
Hif1a_Fw	CCTGCACTGAATCAAGAGGTTGC
Hif1a_Rv	CCATCAGAAGGACTTGCTGGCT
Ppia_Fw	GAGCTCTGAGCACTGGAGAGA
Ppia_Rv	CCACCCTGGCACATGAAT

424
425 **Generation of chimeric embryos**
426 Chimeric embryos were generated following a previous publish protocol (Eakin & Hadjantonakis, 2006).
427 Briefly, wild-type, E-cadherin GFP or mTmG 8-cell stage embryos were transfer to micro-drops of M2 after
428 aneuploid treatment. Zona pellucida was removed by treatment with acidic Tyrode's solution (Sigma,
429 T1788). The embryos were then incubated in Ca2+/Mg2+-free M2 (made in house) for 5 min and then
430 disaggregated into individual blastomeres by gentle mouth pipetting. Mosaic chimeras were form by
431 aggregation of four and four (1:1) of each treatment. Low mosaicism DMSO/AZ3146-treated blastomeres
432 (1:1). Whereas medium mosaicism Reversine/AZ3146-treated blastomeres (1:1). Culture of the chimeras
433 were performed under normoxic and hypoxia condition in KSOM for 48 h to reach blastocyst stage.

434 **Statistical analysis**
435 The statistical tests used are indicated in the corresponding figure legends. Calculations were carried out
436 in Microsoft Excel and data analysis and visualization in Prism 9 software. All graphs show mean values,
437 error bars: s.e.m.

AUTHOR CONTRIBUTIONS

E.S.V designed and conducted the experiments; analyzed and interpreted the data. E.S.V and M.Z.G conceived the project. M.E.B and M.Z.G supervised the study.

ACKNOWLEDGEMENTS

This work was supported by M.Z.G' National Institutes of Health R01 (R01HD101489) grant. E.S.V. is supported by a Pew Latin America fellowship. We thank the Life Science Editors and the Life Science Editors Foundation for invaluable comments and suggestions on the manuscript, and Ariane Helou for copy editing. Data analysis was performed in the Biological Imaging Facility, with the support of the Caltech Beckman Institute and the Arnold and Mabel Beckman Foundation.

DECLARATION OF INTERESTS

The authors declare that they have no conflicts of interest.

REFERENCES

Abuetabh, Y., Wu, H. H., Chai, C., Al Yousef, H., Persad, S., Sergi, C. M., & Leng, R. (2022). DNA damage response revisited: the p53 family and its regulators provide endless cancer therapy opportunities. *Exp Mol Med*, *54*(10), 1658-1669. https://doi.org/10.1038/s12276-022-00863-4

Allais, A., & FitzHarris, G. (2022). Absence of a robust mitotic timer mechanism in early preimplantation mouse embryos leads to chromosome instability. *Development*, *149*(13). https://doi.org/10.1242/dev.200391

Ban, H. S., Kim, B. K., Lee, H., Kim, H. M., Harmalkar, D., Nam, M., Park, S. K., Lee, K., Park, J. T., Kim, I., Lee, K., Hwang, G. S., & Won, M. (2017). The novel hypoxia-inducible factor-1alpha inhibitor IDF-11774 regulates cancer metabolism, thereby suppressing tumor growth. *Cell Death Dis*, *8*(6), e2843. https://doi.org/10.1038/cddis.2017.235

Bermejo-Alvarez, P., Park, K. E., & Telugu, B. P. (2014). Utero-tubal embryo transfer and vasectomy in the mouse model. *J Vis Exp*(84), e51214. https://doi.org/10.3791/51214

Bolton, H., Graham, S. J. L., Van der Aa, N., Kumar, P., Theunis, K., Fernandez Gallardo, E., Voet, T., & Zernicka-Goetz, M. (2016). Mouse model of chromosome mosaicism reveals lineage-specific depletion of aneuploid cells and normal developmental potential. *Nat Commun*, *7*, 11165. https://doi.org/10.1038/ncomms11165

Capalbo, A., Poli, M., Rienzi, L., Girardi, L., Patassini, C., Fabiani, M., Cimadomo, D., Benini, F., Farcomeni, A., Cuzzi, J., Rubio, C., Albani, E., Sacchi, L., Vaiarelli, A., Figliuzzi, M., Findikli, N., Coban, O., Boynukalin, F. K., Vogel, I., . . . Simon, C. (2021). Mosaic human preimplantation embryos and their developmental potential in a prospective, non-selection clinical trial. *Am J Hum Genet*, *108*(12), 2238-2247. https://doi.org/10.1016/j.ajhg.2021.11.002

Choi, J., Kim, W., Yoon, H., Lee, J., & Jun, J. H. (2021). Dynamic Oxygen Conditions Promote the Translocation of HIF-1alpha to the Nucleus in Mouse Blastocysts. *Biomed Res Int*, *2021*, 5050527. https://doi.org/10.1155/2021/5050527

Christodoulou, N., Weberling, A., Strathdee, D., Anderson, K. I., Timpson, P., & Zernicka-Goetz, M. (2019). Morphogenesis of extra-embryonic tissues directs the remodelling of the mouse embryo at implantation. *Nat Commun*, *10*(1), 3557. https://doi.org/10.1038/s41467-019-11482-5

Ciray, H. N., Aksoy, T., Yaramanci, K., Karayaka, I., & Bahceci, M. (2009). In vitro culture under physiologic oxygen concentration improves blastocyst yield and quality: a prospective randomized survey on sibling oocytes. *Fertil Steril*, *91*(4 Suppl), 1459-1461. https://doi.org/10.1016/j.fertnstert.2008.07.1707

485 Currie, C. E., Ford, E., Benham Whyte, L., Taylor, D. M., Mihalas, B. P., Erent, M., Marston, A. L.,
486 Hartshorne, G. M., & McAinsh, A. D. (2022). The first mitotic division of human embryos is highly
487 error prone. *Nat Commun*, *13*(1), 6755. https://doi.org/10.1038/s41467-022-34294-6
488 D'Alise, A. M., Amabile, G., Iovino, M., Di Giorgio, F. P., Bartiromo, M., Sessa, F., Villa, F., Musacchio, A.,
489 & Cortese, R. (2008). Reversine, a novel Aurora kinases inhibitor, inhibits colony formation of
490 human acute myeloid leukemia cells. *Mol Cancer Ther*, *7*(5), 1140-1149.
491 https://doi.org/10.1158/1535-7163.MCT-07-2051
492 Dahdouh, E. M., & Garcia-Velasco, J. A. (2021). Embryos with mosaic results: busting the myth! *Reprod*
493 *Biomed Online*, *43*(1), 1-2. https://doi.org/10.1016/j.rbmo.2021.04.015
494 Eakin, G. S., & Hadjantonakis, A. K. (2006). Production of chimeras by aggregation of embryonic stem
495 cells with diploid or tetraploid mouse embryos. *Nat Protoc*, *1*(3), 1145-1153.
496 https://doi.org/10.1038/nprot.2006.173
497 Goolam, M., Scialdone, A., Graham, S. J. L., Macaulay, I. C., Jedrusik, A., Hupalowska, A., Voet, T.,
498 Marioni, J. C., & Zernicka-Goetz, M. (2016). Heterogeneity in Oct4 and Sox2 Targets Biases Cell
499 Fate in 4-Cell Mouse Embryos. *Cell*, *165*(1), 61-74. https://doi.org/10.1016/j.cell.2016.01.047
500 Greco, E., Minasi, M. G., & Fiorentino, F. (2015). Healthy Babies after Intrauterine Transfer of Mosaic
501 Aneuploid Blastocysts. *N Engl J Med*, *373*(21), 2089-2090.
502 https://doi.org/10.1056/NEJMc1500421
503 Gu, Y., Shen, X., Zhou, D., Wang, Z., Zhang, N., Shan, Z., Jin, L., & Lei, L. (2014). Selection and
504 expression profiles of reference genes in mouse preimplantation embryos of different ploidies at
505 various developmental stages. *PLoS One*, *9*(6), e98956.
506 https://doi.org/10.1371/journal.pone.0098956
507 Hewitt, L., Tighe, A., Santaguida, S., White, A. M., Jones, C. D., Musacchio, A., Green, S., & Taylor, S. S.
508 (2010). Sustained Mps1 activity is required in mitosis to recruit O-Mad2 to the Mad1-C-Mad2 core
509 complex. *J Cell Biol*, *190*(1), 25-34. https://doi.org/10.1083/jcb.201002133
510 Hirakata, C., Lima, K., De Almeida, B. O., De Miranda, L. B. L., Florencio, K. G. D., Furtado, L. C., Costa-
511 Lotufo, L. V., & Machado-Neto, J. A. (2021). Targeting glioma cells by antineoplastic activity of
512 reversine. *Oncol Lett*, *22*(2), 610. https://doi.org/10.3892/ol.2021.12871
513 Houghton, F. D. (2021). HYPOXIA AND REPRODUCTIVE HEALTH: Hypoxic regulation of
514 preimplantation embryos: lessons from human embryonic stem cells. *Reproduction*, *161*(1), F41-
515 F51. https://doi.org/10.1530/REP-20-0322
516 Hu, C. J., Wang, L. Y., Chodosh, L. A., Keith, B., & Simon, M. C. (2003). Differential roles of hypoxia-
517 inducible factor 1alpha (HIF-1alpha) and HIF-2alpha in hypoxic gene regulation. *Mol Cell Biol*,
518 *23*(24), 9361-9374. https://doi.org/10.1128/MCB.23.24.9361-9374.2003
519 Iyer, N. V., Kotch, L. E., Agani, F., Leung, S. W., Laughner, E., Wenger, R. H., Gassmann, M., Gearhart,
520 J. D., Lawler, A. M., Yu, A. Y., & Semenza, G. L. (1998). Cellular and developmental control of
521 O2 homeostasis by hypoxia-inducible factor 1 alpha. *Genes Dev*, *12*(2), 149-162.
522 https://doi.org/10.1101/gad.12.2.149
523 Lan, W., & Cleveland, D. W. (2010). A chemical tool box defines mitotic and interphase roles for Mps1
524 kinase. *J Cell Biol*, *190*(1), 21-24. https://doi.org/10.1083/jcb.201006080
525 Lee, K., & Kim, H. M. (2011). A novel approach to cancer therapy using PX-478 as a HIF-1alpha inhibitor.
526 *Arch Pharm Res*, *34*(10), 1583-1585. https://doi.org/10.1007/s12272-011-1021-3
527 Marti, J. M., Garcia-Diaz, A., Delgado-Bellido, D., O'Valle, F., Gonzalez-Flores, A., Carlevaris, O.,
528 Rodriguez-Vargas, J. M., Ame, J. C., Dantzer, F., King, G. L., Dziedzic, K., Berra, E., de Alava,
529 E., Amaral, A. T., Hammond, E. M., & Oliver, F. J. (2021). Selective modulation by PARP-1 of
530 HIF-1alpha-recruitment to chromatin during hypoxia is required for tumor adaptation to hypoxic
531 conditions. *Redox Biol*, *41*, 101885. https://doi.org/10.1016/j.redox.2021.101885
532 McCoy, R. C. (2017). Mosaicism in Preimplantation Human Embryos: When Chromosomal Abnormalities
533 Are the Norm. *Trends Genet*, *33*(7), 448-463. https://doi.org/10.1016/j.tig.2017.04.001
534 Meuter, A., Rogmann, L. M., Winterhoff, B. J., Tchkonia, T., Kirkland, J. L., & Morbeck, D. E. (2014).
535 Markers of cellular senescence are elevated in murine blastocysts cultured in vitro: molecular
536 consequences of culture in atmospheric oxygen. *J Assist Reprod Genet*, *31*(10), 1259-1267.
537 https://doi.org/10.1007/s10815-014-0299-8
538 Mole, M. A., Weberling, A., & Zernicka-Goetz, M. (2020). Comparative analysis of human and mouse
539 development: From zygote to pre-gastrulation. *Curr Top Dev Biol*, *136*, 113-138.
540 https://doi.org/10.1016/bs.ctdb.2019.10.002

541 Muzumdar, M. D., Tasic, B., Miyamichi, K., Li, L., & Luo, L. (2007). A global double-fluorescent Cre
542 reporter mouse. *Genesis*, *45*(9), 593-605. https://doi.org/10.1002/dvg.20335
543 Nakamura, H., Sekine, H., Kato, H., Masai, H., Gradin, K., & Poellinger, L. (2022). Hypoxia-inducible
544 factor-1alpha and poly [ADP ribose] polymerase 1 cooperatively regulate Notch3 expression
545 under hypoxia via a noncanonical mechanism. *J Biol Chem*, *298*(7), 102137.
546 https://doi.org/10.1016/j.jbc.2022.102137
547 Nguyen, A. Q., Bardua, I., Greene, B., Wrenzycki, C., Wagner, U., & Ziller, V. (2020). Mouse embryos
548 exposed to oxygen concentrations that mimic changes in the oviduct and uterus show
549 improvement in blastocyst rate, blastocyst size, and accelerated cell division. *Reprod Biol*, *20*(2),
550 147-153. https://doi.org/10.1016/j.repbio.2020.03.011
551 Palmerola, K. L., Amrane, S., De Los Angeles, A., Xu, S., Wang, N., de Pinho, J., Zuccaro, M. V.,
552 Taglialatela, A., Massey, D. J., Turocy, J., Robles, A., Subbiah, A., Prosser, B., Lobo, R., Ciccia,
553 A., Koren, A., Baslan, T., & Egli, D. (2022a). Replication stress impairs chromosome segregation
554 and preimplantation development in human embryos. *Cell*.
555 https://doi.org/10.1016/j.cell.2022.06.028
556 Palmerola, K. L., Amrane, S., De Los Angeles, A., Xu, S., Wang, N., de Pinho, J., Zuccaro, M. V.,
557 Taglialatela, A., Massey, D. J., Turocy, J., Robles, A., Subbiah, A., Prosser, B., Lobo, R., Ciccia,
558 A., Koren, A., Baslan, T., & Egli, D. (2022b). Replication stress impairs chromosome segregation
559 and preimplantation development in human embryos. *Cell*, *185*(16), 2988-3007 e2920.
560 https://doi.org/10.1016/j.cell.2022.06.028
561 Pauerova, T., Radonova, L., Kovacovicova, K., Novakova, L., Skultety, M., & Anger, M. (2020).
562 Aneuploidy during the onset of mouse embryo development. *Reproduction*, *160*(5), 773-782.
563 https://doi.org/10.1530/REP-20-0086
564 Pietrzak, J., Spickett, C. M., Ploszaj, T., Virag, L., & Robaszkiewicz, A. (2018). PARP1 promoter links cell
565 cycle progression with adaptation to oxidative environment. *Redox Biol*, *18*, 1-5.
566 https://doi.org/10.1016/j.redox.2018.05.017
567 Santaguida, S., Tighe, A., D'Alise, A. M., Taylor, S. S., & Musacchio, A. (2010). Dissecting the role of
568 MPS1 in chromosome biorientation and the spindle checkpoint through the small molecule
569 inhibitor reversine. *J Cell Biol*, *190*(1), 73-87. https://doi.org/10.1083/jcb.201001036
570 Shahbazi, M. N., Wang, T., Tao, X., Weatherbee, B. A. T., Sun, L., Zhan, Y., Keller, L., Smith, G. D.,
571 Pellicer, A., Scott, R. T., Jr., Seli, E., & Zernicka-Goetz, M. (2020). Developmental potential of
572 aneuploid human embryos cultured beyond implantation. *Nat Commun*, *11*(1), 3987.
573 https://doi.org/10.1038/s41467-020-17764-7
574 Simoes-Sousa, S., Littler, S., Thompson, S. L., Minshall, P., Whalley, H., Bakker, B., Belkot, K., Moralli,
575 D., Bronder, D., Tighe, A., Spierings, D. C. J., Bah, N., Graham, J., Nelson, L., Green, C. M.,
576 Foijer, F., Townsend, P. A., & Taylor, S. S. (2018). The p38alpha Stress Kinase Suppresses
577 Aneuploidy Tolerance by Inhibiting Hif-1alpha. *Cell Rep*, *25*(3), 749-760 e746.
578 https://doi.org/10.1016/j.celrep.2018.09.060
579 Singla, S., Iwamoto-Stohl, L. K., Zhu, M., & Zernicka-Goetz, M. (2020). Autophagy-mediated apoptosis
580 eliminates aneuploid cells in a mouse model of chromosome mosaicism. *Nat Commun*, *11*(1),
581 2958. https://doi.org/10.1038/s41467-020-16796-3
582 Soto, M., Raaijmakers, J. A., Bakker, B., Spierings, D. C. J., Lansdorp, P. M., Foijer, F., & Medema, R. H.
583 (2017). p53 Prohibits Propagation of Chromosome Segregation Errors that Produce Structural
584 Aneuploidies. *Cell Rep*, *19*(12), 2423-2431. https://doi.org/10.1016/j.celrep.2017.05.055
585 Starostik, M. R., Sosina, O. A., & McCoy, R. C. (2020). Single-cell analysis of human embryos reveals
586 diverse patterns of aneuploidy and mosaicism. *Genome Res*, *30*(6), 814-825.
587 https://doi.org/10.1101/gr.262774.120
588 Thompson, S. L., & Compton, D. A. (2010). Proliferation of aneuploid human cells is limited by a p53-
589 dependent mechanism. *J Cell Biol*, *188*(3), 369-381. https://doi.org/10.1083/jcb.200905057
590 Vanneste, E., Voet, T., Le Caignec, C., Ampe, M., Konings, P., Melotte, C., Debrock, S., Amyere, M.,
591 Vikkula, M., Schuit, F., Fryns, J. P., Verbeke, G., D'Hooghe, T., Moreau, Y., & Vermeesch, J. R.
592 (2009). Chromosome instability is common in human cleavage-stage embryos. *Nat Med*, *15*(5),
593 577-583. https://doi.org/10.1038/nm.1924
594 Vazquez-Diez, C., Paim, L. M. G., & FitzHarris, G. (2019). Cell-Size-Independent Spindle Checkpoint
595 Failure Underlies Chromosome Segregation Error in Mouse Embryos. *Curr Biol*, *29*(5), 865-873
596 e863. https://doi.org/10.1016/j.cub.2018.12.042

597 Zhao, T., Ren, H., Jia, L., Chen, J., Xin, W., Yan, F., Li, J., Wang, X., Gao, S., Qian, D., Huang, C., &
598 Hao, J. (2015). Inhibition of HIF-1alpha by PX-478 enhances the anti-tumor effect of gemcitabine
599 by inducing immunogenic cell death in pancreatic ductal adenocarcinoma. *Oncotarget*, *6*(4),
600 2250-2262. https://doi.org/10.18632/oncotarget.2948
601 Zhu, J., Tsai, H. J., Gordon, M. R., & Li, R. (2018). Cellular Stress Associated with Aneuploidy. *Dev Cell*,
602 *44*(4), 420-431. https://doi.org/10.1016/j.devcel.2018.02.002
603 Zhu, M., Shahbazi, M., Martin, A., Zhang, C., Sozen, B., Borsos, M., Mandelbaum, R. S., Paulson, R. J.,
604 Mole, M. A., Esbert, M., Titus, S., Scott, R. T., Campbell, A., Fishel, S., Gradinaru, V., Zhao, H.,
605 Wu, K., Chen, Z. J., Seli, E., . . . Zernicka Goetz, M. (2021). Human embryo polarization requires
606 PLC signaling to mediate trophectoderm specification. *Elife*, *10*.
607 https://doi.org/10.7554/eLife.65068
608 Zhu, M., & Zernicka-Goetz, M. (2020). Principles of Self-Organization of the Mammalian Embryo. *Cell*,
609 *183*(6), 1467-1478. https://doi.org/10.1016/j.cell.2020.11.003
610

611 **FIGURES AND FIGURE LEGENDS**

612 Figure 1| **Lineage analysis of aneuploid embryos generated by selective Mps1 inhibitors AZ3146 and**
613 **reversine.**

614 (A) Graphic representation of 4-cell embryos treated with DMSO (control) or Mps1 inhibitors reversine (0.5
615 μM) and AZ3146 (20 μM) to inactivate the spindle assembly checkpoint (SAC) and induce chromosome
616 segregation errors. After washing, embryos were cultured to the mature blastocyst stage (E4.5) and
617 analyzed for lineage specification. (B) Immunofluorescence imaging of well-known lineage markers CDX2
618 (TE), NANOG (EPI) and SOX17 (PE) reveals that overall embryonic morphology and cavitation is not
619 affected by Mps1 inhibition. (C) Number of cells in each lineage was quantified to evaluate the effect of
620 drug treatment on blastocyst development. Importantly, both reversine and AZ3146-treatments reduce the
621 number of cells in the ICM, marked by NANOG (EPI) and SOX17 (PE). Whereas the TE, marked by CDX2,
622 is reduced only in the reversine-treated embryos. (n=28 embryos per treatment, cumulative of three
623 independent experiments) (***P<0.0002, **P<0.01, *P<0.05, Mann–Whitney U-test, error bars represent
624 s.e.m). (D) Analysis of DNA damage and DNA repair based on immunofluorescence against γH2A.X
625 (phosphorylated form of H2A.X, white) and PARP1 (red), respectively. (E) Intensity analysis shows that
626 reversine and AZ3146 increase DNA damage at the 8-cell stage through morula stage compared with
627 DMSO-treated embryos. Importantly, reversine appears to downregulate PARP1 expression at the 8-cell
628 stage, which extends to morula stage embryos (***P<0.0004, **P<0.01, *P<0.05, t-test, error bars represent
629 s.e.m).
630

631 Figure 2 | **AZ3146-treated embryos elevate HIF1A activity to support formation of the TE and PE.**

632 A) qPCR analysis of *p53* and *Hif1a* mRNA expression at morula and blastocyst stages reveals that *p53* is
633 upregulated in reversine-treated embryos and that *Hif1a* is upregulated in AZ3146-treated embryos at
634 morula stages; 3 biological replicates and 2 technical replicates per experiment with each replicate having
635 a minimum of 16 embryos (**P<0.01, *P<0.05, Welch's t-test). B) Immunofluorescence against HIF1A
636 (black) shows an increase in nuclear intensity in AZ3146-treated embryos at morula stages. At blastocyst
637 stage, nuclear and cytoplasmic HIF1A are increased in AZ3146-treated embryos; normalization was based
638 on DAPI staining (magenta). (****P<0.0001, **P<0.01, *P<0.05, Mann–Whitney U-test, error bars represent

639 s.e.m) (C) Graphic representation of 4-cell embryos treated with DMSO and aneuploid drugs.
640 Downregulation of HIF1A was achieved by treatment with IDF-11774 immediately after wash of the
641 aneuploid drugs. Immunofluorescence analysis of lineage specification in blastocyst cultured with the
642 HIF1A inhibitor IDF-11774 using antibodies against CDX2 (TE), NANOG (EPI) and SOX17 (PE).
643 Importantly, IDF-11774 appears to affect cavitation of some AZ3146-treated embryos. (D) Lineage analysis
644 at the blastocyst stage shows that TE and PE specification are affected by IDF-11774 treatment. Number
645 of cells in each lineage was quantified to evaluate the effect on blastocyst development. (****P<0.0001,
646 **P<0.01, *P<0.05, Mann–Whitney U-test, error bars represent s.e.m. n=20 embryos per treatment
647 collected from 3 independent experiments).
648
649 Figure 3 | **Hypoxia exposure reduces DNA damage and affects lineage proportions in the aneuploid**
650 **blastocyst.**
651 (A) Graphic representation of the hypoxia experiments. 2-cell embryos were cultured until the blastocyst
652 stage in hypoxia conditions (5% oxygen). As before, 4-cell stage embryos were treated with DMSO or Mps1
653 inhibitors reversine and AZ3146 until the 8-cell stage. After washing, embryos were cultured to the mature
654 blastocyst stage (E4.5) and analyzed for lineage specification. (B) Immunofluorescence imaging of well-
655 known lineage markers CDX2 (TE), NANOG (EPI) and SOX17 (PE) reveals that overall embryonic
656 morphology and cavitation is not affected by Mps1 inhibition or hypoxia. (C) Lineage analysis at blastocyst
657 stage. Number of cells in each lineage was used to evaluate the effects in blastocyst development.
658 (****P<0.0001, *P<0.05, Mann–Whitney U-test, error bars represent s.e.m, n=18 embryos per treatment
659 collected from 3 independent experiments). (D) Immunofluorescence against PARP1 (red) and γH2A.X
660 (white) in blastocyst after drug treatments. (E) Intensity analysis shows that, under hypoxia, at 8-cell stage,
661 DNA damage is increased after exposure to reversine but not AZ3146. PARP1 expression is altered only
662 at the 8-cell stage in reversine-treated embryos (***P<0.0004, **P<0.01, *P<0.05, t-test, error bars
663 represent s.e.m. n=25 embryos per treatment collected from 3 independent experiments).
664
665 Figure 4 | **Hypoxia affects cell competition between diploid and aneuploid cells during pre-**
666 **implantation development.** (A) Graphic representation of the cell competition experiments. Embryos were
667 treated at the 4-cell stage with DMSO or Mps1 inhibitors reversine and AZ3146. After washing, 8-cell stage
668 embryos were disaggregated, and re-aggregated to form chimeras containing a 1:1 ratio of DMSO/AZ314-
669 treated blastomeres and Reversine/AZ314-treated blastomeres. Following aggregation, chimeras were
670 cultured to the mature blastocyst stage (E4.5) and analyzed for lineage specification. For identification of
671 the treatment, we use transgenics lines with membrane markers. Immunofluorescence for CDX2, NANOG,
672 and SOX17 was performed to test lineage specification and allocation during (B) normoxia and (C) hypoxia.
673 Lineage allocation quantification was based on the above markers. Importantly, D) in normoxia, both
674 chimeras have the same number of cells in all the lineages except the EPI. In addition, AZ3146-treated
675 blastomeres outcompete reversine-treated blastomeres in medium-grade mosaics in the TE and the EPI.

676 E) Under hypoxia, both chimeras have similar number of cells in all the lineages. Yet, AZ3146-blastomeres
677 do not outcompete reversine-treated blastomeres. Quantification of the contribution of AZ3146-treated
678 blastomeres to the chimeras showed that, (F) under normoxia, compare with DMSO-treated cells, no
679 preferential allocation of aneuploid cells occurs in the TE. In contrast, AZ3146-treated blastomeres
680 increased their contribution when compare with reversine- treated blastomeres, but only significantly on the
681 EPI and the PE. (G) During hypoxia, DMSO/AZ3146 chimeras did not change their behavior. Confirming a
682 preferential allocation of diploid cells to the EPI. In Reversine/AZ3146 chimeras, AZ3146-treated
683 blastomeres contribute similarly to reversine-blastomeres to the TE and PE but significantly increase
684 contribution to the EPI. These results indicate that hypoxia favors the survival of reversine-induced
685 aneuploid cells (****P<0.00001, **P<0.01, *P<0.05, Mann–Whitney U-test, error bars represent s.e.m, n>7
686 embryos per treatment collected from 3 independent experiments).
687
688 Figure 5| **HIF1A inhibition increases the proportion of euploid cells in mosaic embryos.** (A) Schematic
689 of HIF1A inhibition by IDF-11774 in 8-cell stage aggregation chimeras cultured in hypoxia.
690 Immunofluorescence for CDX2, NANOG, and SOX17 was performed to test lineage specification and
691 allocation. (B) HIF1A inhibition in low-grade mosaicism does not affect overall morphology but affects (C)
692 cavitation. In contrast, (E) HIF1A inhibition in medium-grade mosaicism affects morphology, and (F)
693 cavitation of the embryos. Lineage allocation quantification after IDF-1174 reveals a significant reduction
694 of total cell number (D) in low-grade mosaicism as well as a reduction in cell number in the TE but not in
695 the EPI and PE. In contrast, total cell number is not affected (G) in medium-grade mosaicism. However,
696 IDF11-774 treatment appears to increase the cell number of the PE. These results show that HIF1A
697 inhibition in hypoxic conditions differentially affect each type of mosaic embryos. (**P<0.005, *P<0.05,
698 Mann–Whitney U-test, error bars represent s.e.m., n>8 embryos per treatment collected from 3
699 independent experiments).
700
701 Figure S.1| **AZ3146-treated embryos are aneuploid and can develop to post-implantation stages.**
702 (A) *In situ* chromosome counting of 8-cell stage embryos after drug treatments. Representative images of
703 individual embryos in the different treatments. DNA (white) is visualized by DAPI staining and kinetochores
704 (red) by CREST antibody. PB (polar body), MN (micronuclei). Each chromosome presents 2 CREST dots.
705 The large number is the cell ID and the smaller number indicates the number of chromosomes, “n”. Diploid
706 blastomeres present 40 pairs of CREST dots. Phalloidin (cyan) was used for cell segmentation. (B)
707 Quantification of the incidence of aneuploid events, designated as those with more than 2 chromosomes
708 (MN>2chr), less than 2 chromosomes (MN<2chr), without kinetochores (MN-CREST) and non-dividing
709 nucleus (ND cell). We observed an increase in MN following reversine and AZ3146 treatment. Importantly,
710 reversine-treated cells have a higher number of ND cells and MN-CREST staining. (n=256 cell DMSO
711 treatment, n=304 cells AZ3146 treatment, n=144 cells reversine treatment, ****P<0.00001, *P<0.05, Mann–
712 Whitney U-test, error bars represent s.e.m). (C) Embryo transfer experiments show higher implantation

events (% decidua formation) in AZ3146-treated embryos. The left uterine horn was used for transfer of reversine-treated blastocyst and the right uterine horn for AZ3146-treated blastocyst. (n=7 embryos transplanted per uterine horn, repeated experiments two times) (D) Only AZ3146-treated blastocyst can develop post-gastrulation E9.5 fetuses (% embryo formation).

Figure S.2| **PARP1 is required for ICM development**.
(A) Immunofluorescence against PARP1 (red) and γH2A.X (white) in blastocyst after drug treatments. Notice accumulation of DNA damage in reversine-treated blastocyst. (B) Immunofluorescence against PARP1 (red), NANOG (white, epiblast) and CDX2 (green, trophectoderm). Analysis of PARP1 intensity shows an increase in the EPI lineage (****P<0.00001, ***P<0.0006, Mann–Whitney U-test, error bars represent s.e.m, n>21 embryos per treatment collected from 3 independent experiments). To confirm these observation, scRNA-seq (Deng et. al 2014) shows enrichment of *Parp1* mRNA specifically in the EPI. (C) Graphic representation of 4-cell embryos treated with DMSO and aneuploid drugs. Downregulation of PARP1 was achieved by treatment with Olaparib from morula to blastocyst stage. (D) Effects of the inhibition of PARP1 function were assessed by immunofluorescence against CDX2 (TE), NANOG (EPI) and SOX17 (PE) in the different treatments. Importantly, Olaparib treatment does not affect blastocyst morphology. (E) Lineage analysis at blastocyst stage shows a specific effect on the survival of epiblast and PE cells in reversine-treated embryos. Ratio of cells in each lineage in the blastocyst is normalized based on DMSO treatment. (*P<0.05, Mann–Whitney U-test, error bars represent s.e.m n=15 embryos per treatment collected from 3 independent experiments).

Figure S.3| **Pharmacological inhibitors of HIF1A have distinct effects on mouse pre-implantation embryos.** (A) Inhibition of HIF1A from zygotes to blastocyst stage with PX-478 or IDF-11774. Immunofluorescence against CDX2 (TE) and DAPI (magenta) was used to assess blastocyst development. Importantly, IDF-11774 does not compromise pre-implantation development, whereas PX-478 compromised the survival and overall morphology of the blastocyst. (B) Analysis of the number of trophectoderm cells (CDX2) and total number (DAPI) shows a deleterious effect of PX-478 during blastocyst development (****P<0.0001, Mann–Whitney U-test, error bars represent s.e.m, n>12 embryos per treatment collected from 3 independent experiments).

Figure S.4| **Correlation plot of AZ3146-treated cells in the epiblast and trophectoderm.** Scatter plot of AZ3146-treated cells in epiblast and trophectoderm in DMSO/AZ3146 and Reversine/AZ3146 mosaic blastocysts cultured under normoxic and hypoxic conditions.

Figure S.5| **Aneuploidies generated before the 2-cell stage does not affect lineage specification in mosaic embryos.** (A) Immunofluorescence for CDX2, NANOG, and SOX17 was performed in blastocysts after zygote treatment with Mps1 inhibitors. Importantly, reversine treatment at zygote stages affects

750 morphology of blastocyst. (B) Lineage analysis of blastocyst shows no effect in AZ3146-treated embryos.
751 Whereas reversine treatment reduces the cell number to almost half. Ratio of cells in each lineage in the
752 blastocyst is normalized based on DMSO treatments. (n>27 embryos per treatment collected from 3
753 independent experiments, ****P<0.0001, *P<0.0044 , Mann–Whitney U-test, error bars represent s.e.m).
754 (C) Aggregation chimeras at 2-cell stage were created by using transgenics lines with membrane markers:
755 mTmG (green) and E-cadherin (white). Subsequently, (D) immunofluorescence for CDX2, NANOG, and
756 SOX17 was performed to quantify lineage allocation. Our results show no effect on embryo morphology in
757 our chimeras. However, reversine/DMSO (D/R) chimeras seems to have increase events of cell extrusion
758 and reversine/AZ3146 chimeras are smaller in number of cells compare with DMSO/AZ3146 chimeras. (E)
759 Data show the proportion of AZ3146-treated cells in DMSO/AZ3146 mosaic blastocysts (grey) and in
760 reversine/AZ3146 mosaic blastocysts (blue), as well as the proportion of reversine-treated cells in
761 DMSO/reversine mosaic blastocysts (red).
762
763 Figure S.6| **IDF-11774-mediated inhibition of HIF1A increases the proportion of euploid cells in**
764 **mosaic embryos.** Brightfield images of low- and medium-mosaic chimeras grown in (A) DMSO and (B)
765 IDF-11774. Quantification of the contribution of AZ3146-treated blastomeres to the chimeras showed that,
766 (C) in DMSO/AZ3146 mosaics, IDF-11774 treatment reduces the proportion of AZ3146-treated
767 blastomeres, whereas (D) in reversine/AZ3146 mosaics, IDF-11774 treatment slightly increases the
768 proportion of AZ3146-treated blastomeres. These results may indicate that HIF1A inhibition impairs the
769 less fit population in chimeric embryos.
770

Figure 1

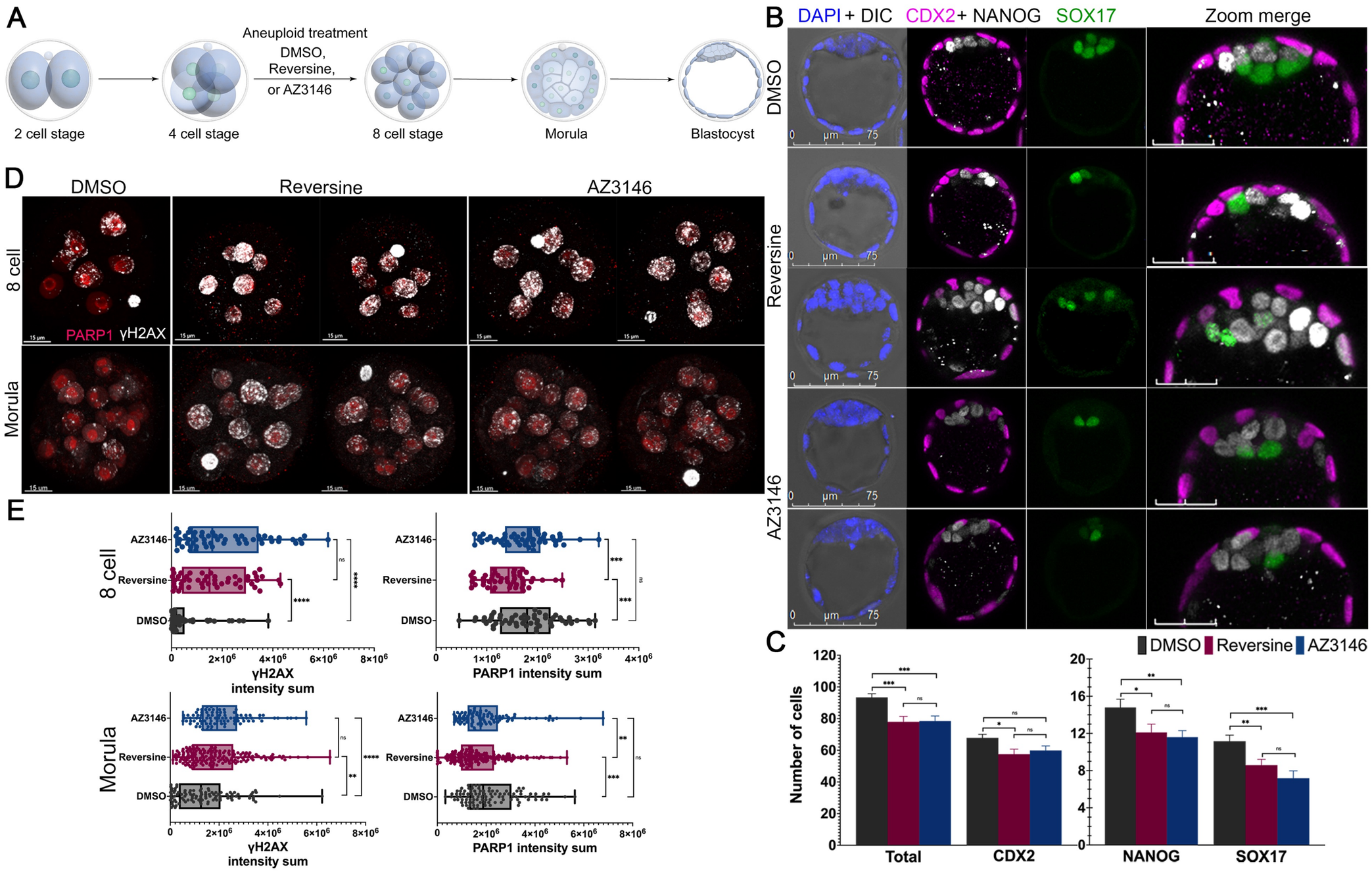
A
Aneuploid treatment
DMSO,
Reversine,
or AZ3146
2 cell stage
4 cell stage
8 cell stage
Morula
Blastocyst
B
DAPI + DIC
CDX2+ NANOG
SOX17
Zoom merge
DMSO
Reversine
AZ3146
C
DMSO
Reversine
AZ3146
Number of cells
Total
CDX2
NANOG
SOX17
D
DMSO
Reversine
AZ3146
8 cell
Morula
PARP1
γH2AX
E
8 cell
Morula
AZ3146
Reversine
DMSO
γH2AX
intensity sum
PARP1 intensity sum

Figure 2

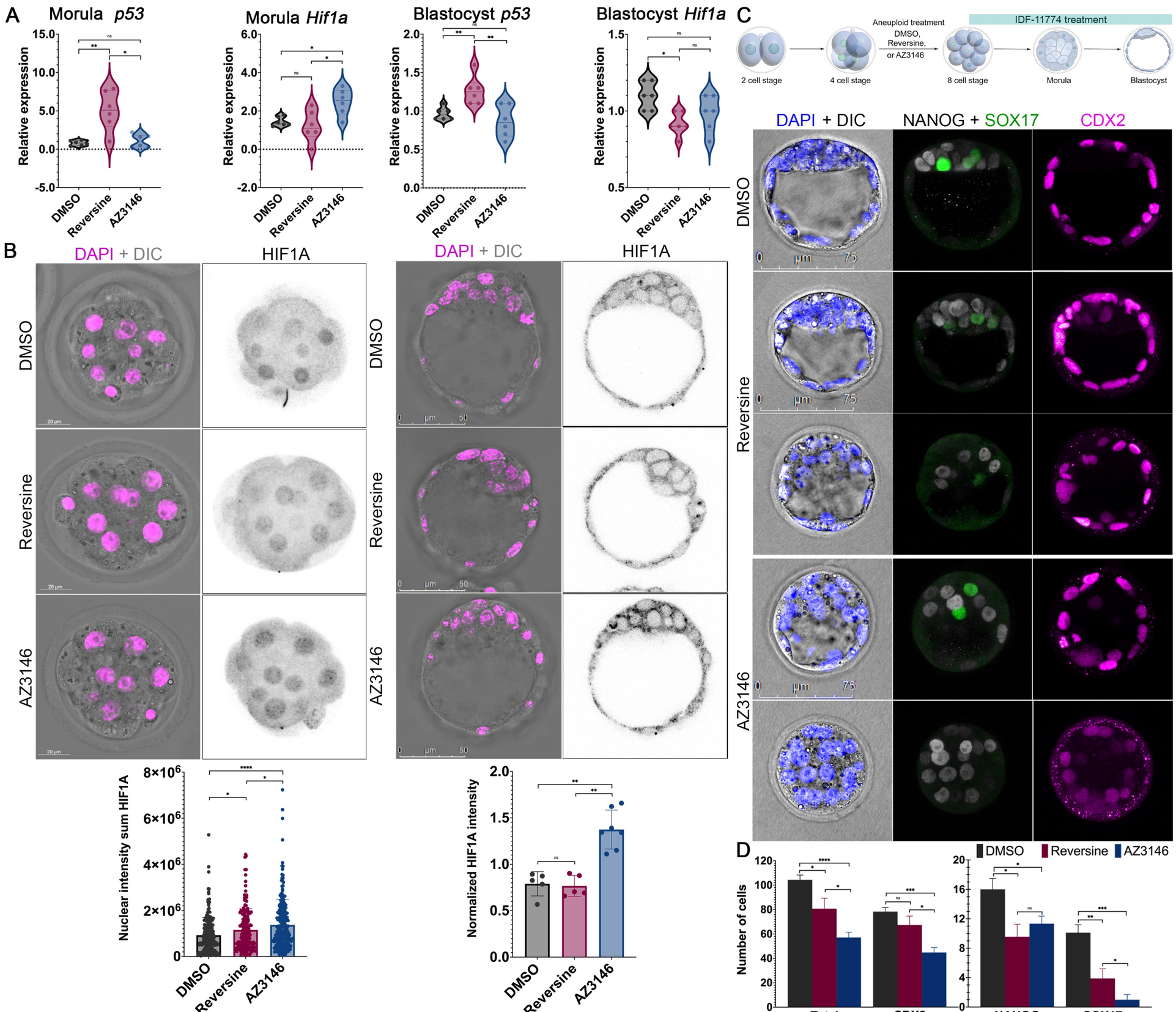
A
Morula p53
Morula Hif1a
Blastocyst p53
Blastocyst Hif1a
Relative expression
DMSO
Reversine
AZ3146
B
DAPI + DIC
HIF1A
DMSO
Reversine
AZ3146
Nuclear intensity sum HIF1A
Normalized HIF1A intensity
C
Aneuploid treatment
DMSO, Reversine, or AZ3146
IDF-11774 treatment
2 cell stage
4 cell stage
8 cell stage
Morula
Blastocyst
DAPI + DIC
NANOG + SOX17
CDX2
D
DMSO
Reversine
AZ3146
Number of cells
Total
CDX2
NANOG
SOX17

Figure 3

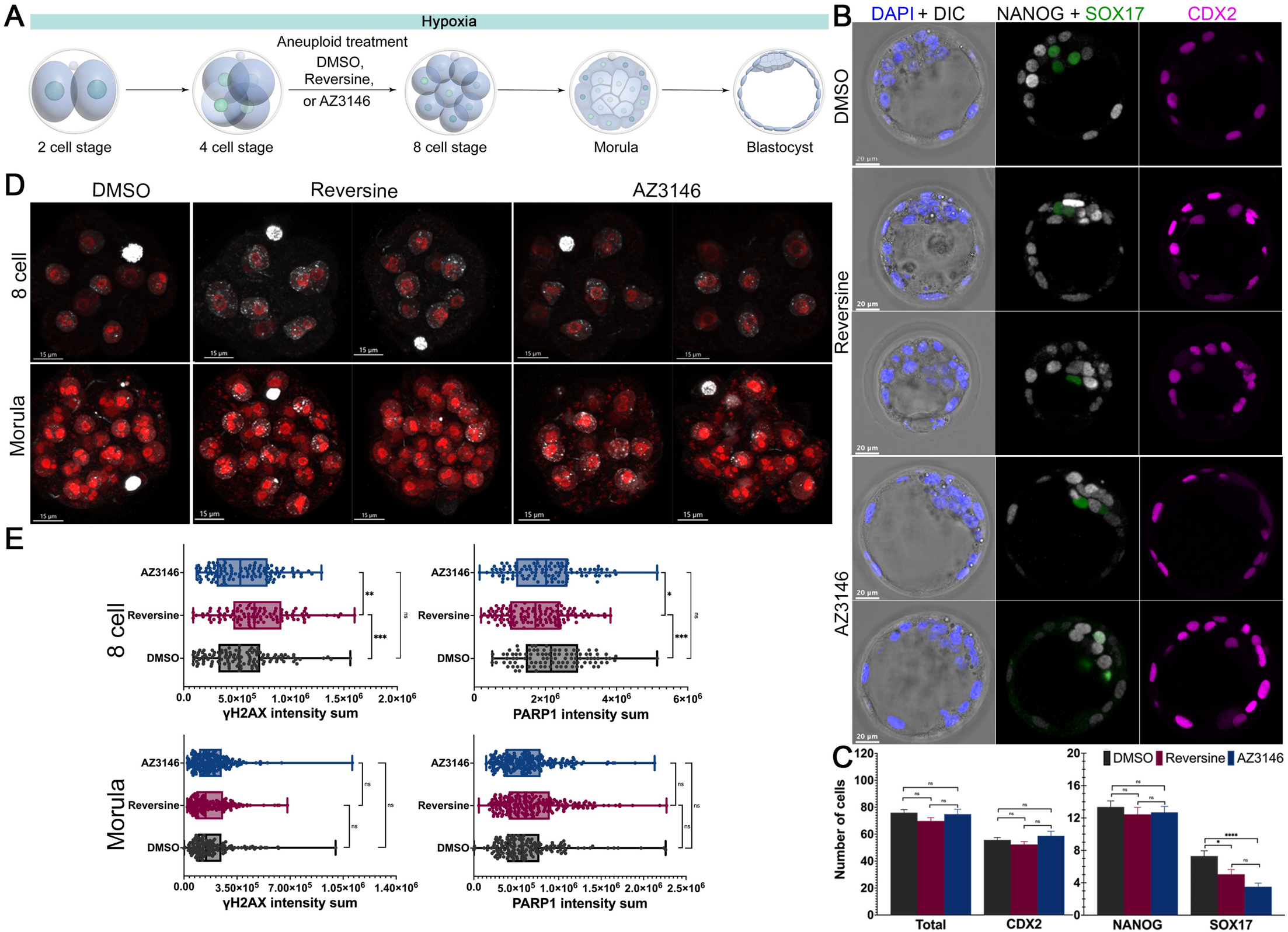
A
Hypoxia
Aneuploid treatment
DMSO,
Reversine,
or AZ3146
2 cell stage
4 cell stage
8 cell stage
Morula
Blastocyst
B
DAPI + DIC
NANOG + SOX17
CDX2
DMSO
Reversine
AZ3146
20 µm
C
DMSO
Reversine
AZ3146
Number of cells
Total
CDX2
NANOG
SOX17
D
DMSO
Reversine
AZ3146
8 cell
Morula
15 µm
E
8 cell
Morula
AZ3146
Reversine
DMSO
γH2AX intensity sum
PARP1 intensity sum
ns

Figure 4

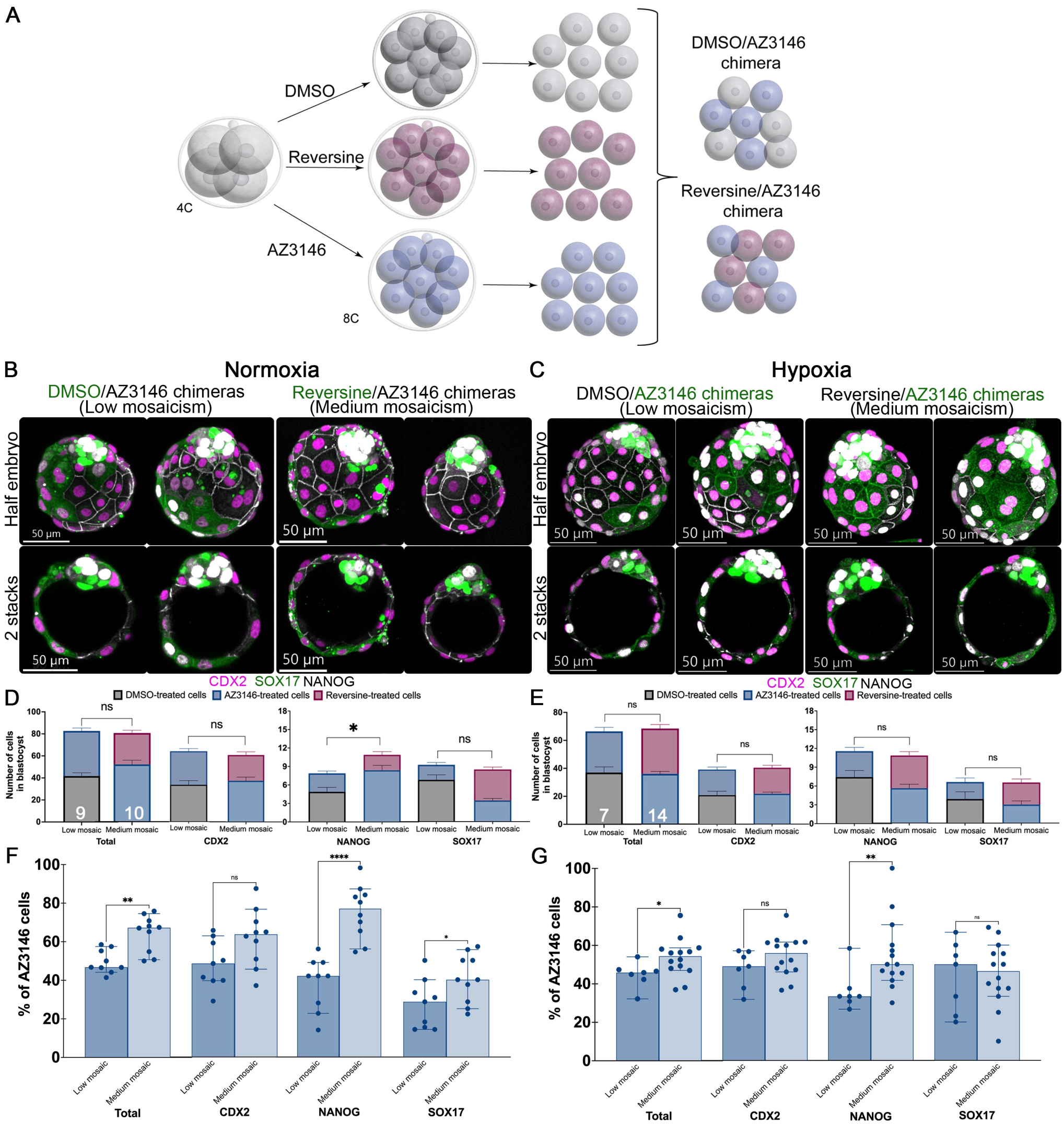
A
DMSO
Reversine
AZ3146
4C
8C
DMSO/AZ3146 chimera
Reversine/AZ3146 chimera
B
Normoxia
DMSO/AZ3146 chimeras (Low mosaicism)
Reversine/AZ3146 chimeras (Medium mosaicism)
Half embryo
2 stacks
50 µm
C
Hypoxia
DMSO/AZ3146 chimeras (Low mosaicism)
Reversine/AZ3146 chimeras (Medium mosaicism)
CDX2 SOX17 NANOG
D
DMSO-treated cells
AZ3146-treated cells
Reversine-treated cells
Number of cells in blastocyst
ns
*
9
10
Low mosaic
Medium mosaic
Total
CDX2
NANOG
SOX17
E
7
14
F
% of AZ3146 cells
**
****
G

Figure 5

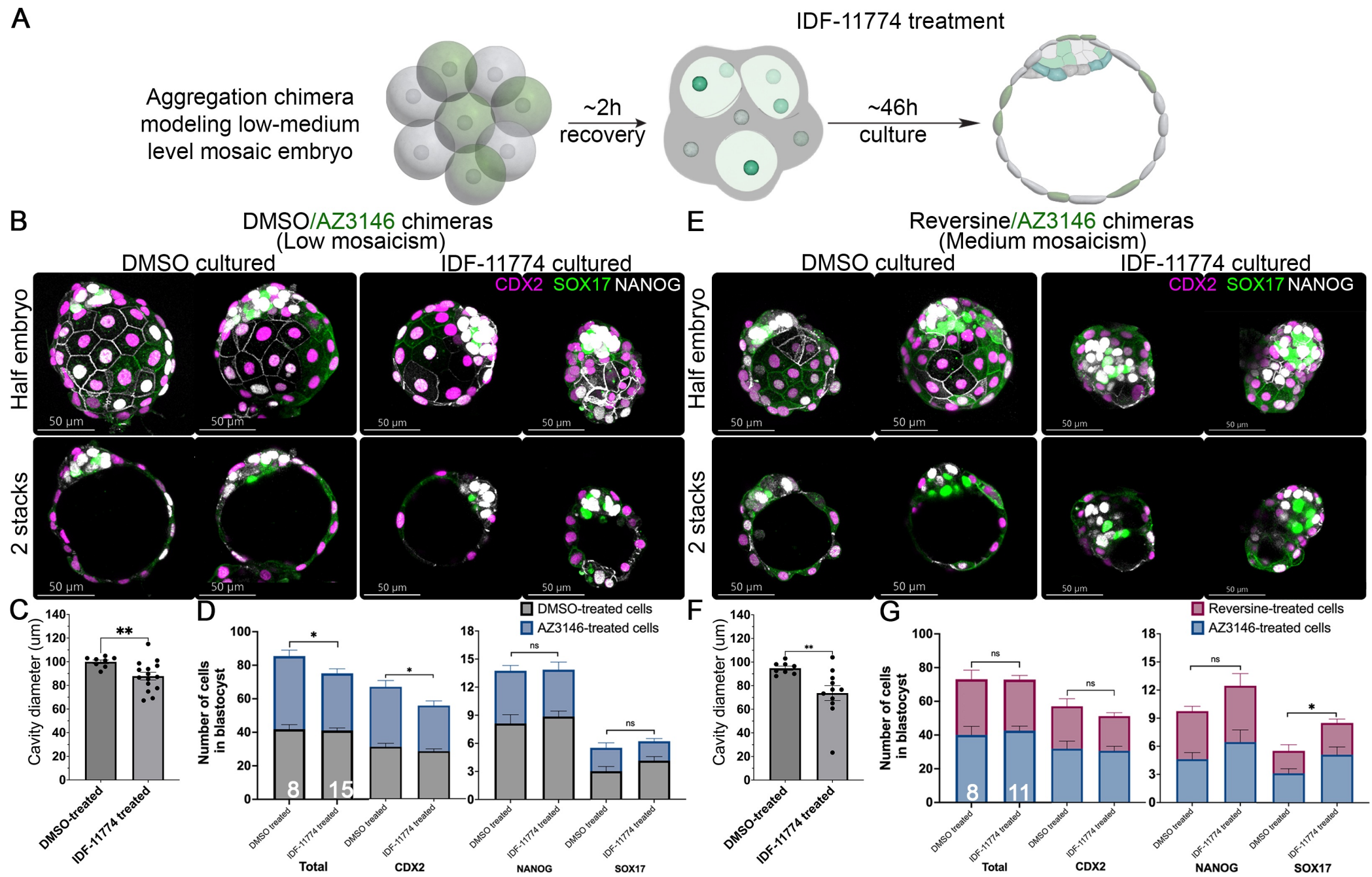
A
IDF-11774 treatment
Aggregation chimera modeling low-medium level mosaic embryo
~2h recovery
~46h culture
B
DMSO/AZ3146 chimeras (Low mosaicism)
DMSO cultured
IDF-11774 cultured
CDX2 SOX17 NANOG
Half embryo
2 stacks
50 µm
E
Reversine/AZ3146 chimeras (Medium mosaicism)
C
Cavity diameter (um)
DMSO-treated
IDF-11774 treated
D
Number of cells in blastocyst
DMSO-treated cells
AZ3146-treated cells
Total
CDX2
NANOG
SOX17
F
G
Reversine-treated cells

Figure S. 1

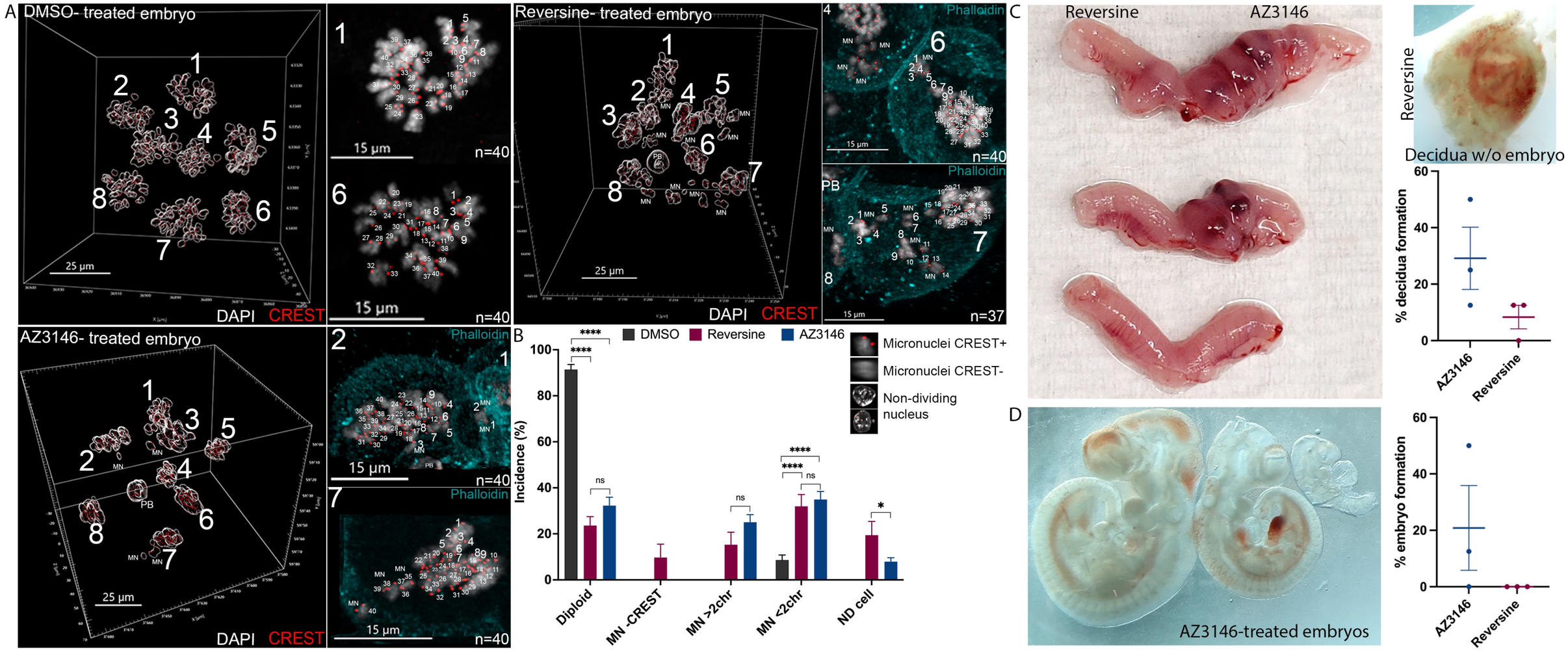
A
DMSO- treated embryo
25 µm
DAPI CREST
15 µm
n=40
Reversine- treated embryo
Phalloidin
n=37
AZ3146- treated embryo
B
DMSO
Reversine
AZ3146
Micronuclei CREST+
Micronuclei CREST-
Non-dividing nucleus
Incidence (%)
Diploid
MN -CREST
MN >2chr
MN <2chr
ND cell
C
Reversine
AZ3146
Decidua w/o embryo
% decidua formation
D
AZ3146-treated embryos
% embryo formation

Figure S.2

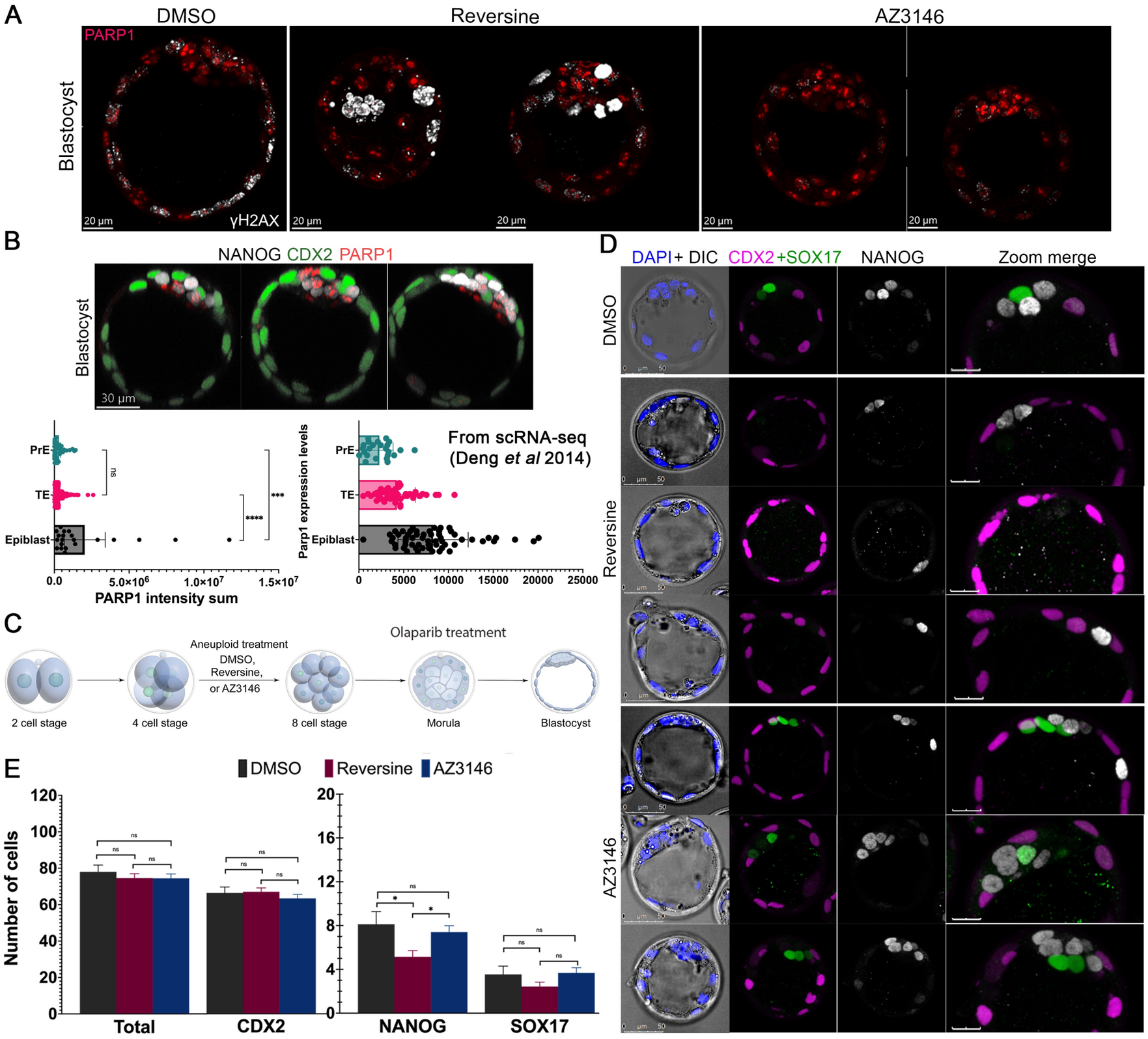
A
DMSO
Reversine
AZ3146
PARP1
Blastocyst
γH2AX
20 µm
B
NANOG CDX2 PARP1
Blastocyst
30 µm
PrE
TE
Epiblast
ns
***
****
0.0
5.0×10^6
1.0×10^7
1.5×10^7
PARP1 intensity sum
Parp1 expression levels
From scRNA-seq
(Deng et al 2014)
0
5000
10000
15000
20000
25000
C
Aneuploid treatment
DMSO,
Reversine,
or AZ3146
Olaparib treatment
2 cell stage
4 cell stage
8 cell stage
Morula
Blastocyst
D
DAPI + DIC
CDX2 +SOX17
NANOG
Zoom merge
DMSO
Reversine
AZ3146
E
DMSO
Reversine
AZ3146
Number of cells
Total
CDX2
NANOG
SOX17
ns
*

Figure S. 3

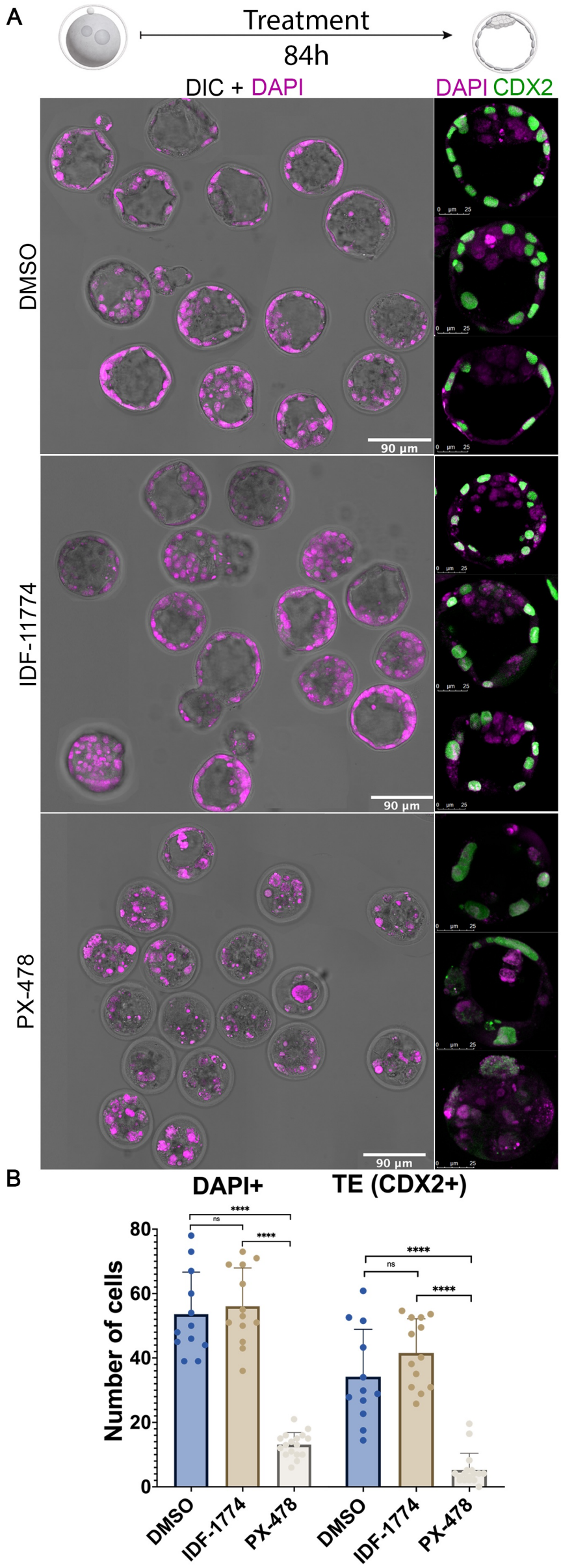
A
Treatment
84h
DIC + DAPI
DAPI CDX2
DMSO
IDF-11774
PX-478
90 µm
B
DAPI+
TE (CDX2+)
Number of cells
80
60
40
20
0
****
ns
DMSO
IDF-1774
PX-478

Figure S. 4

A

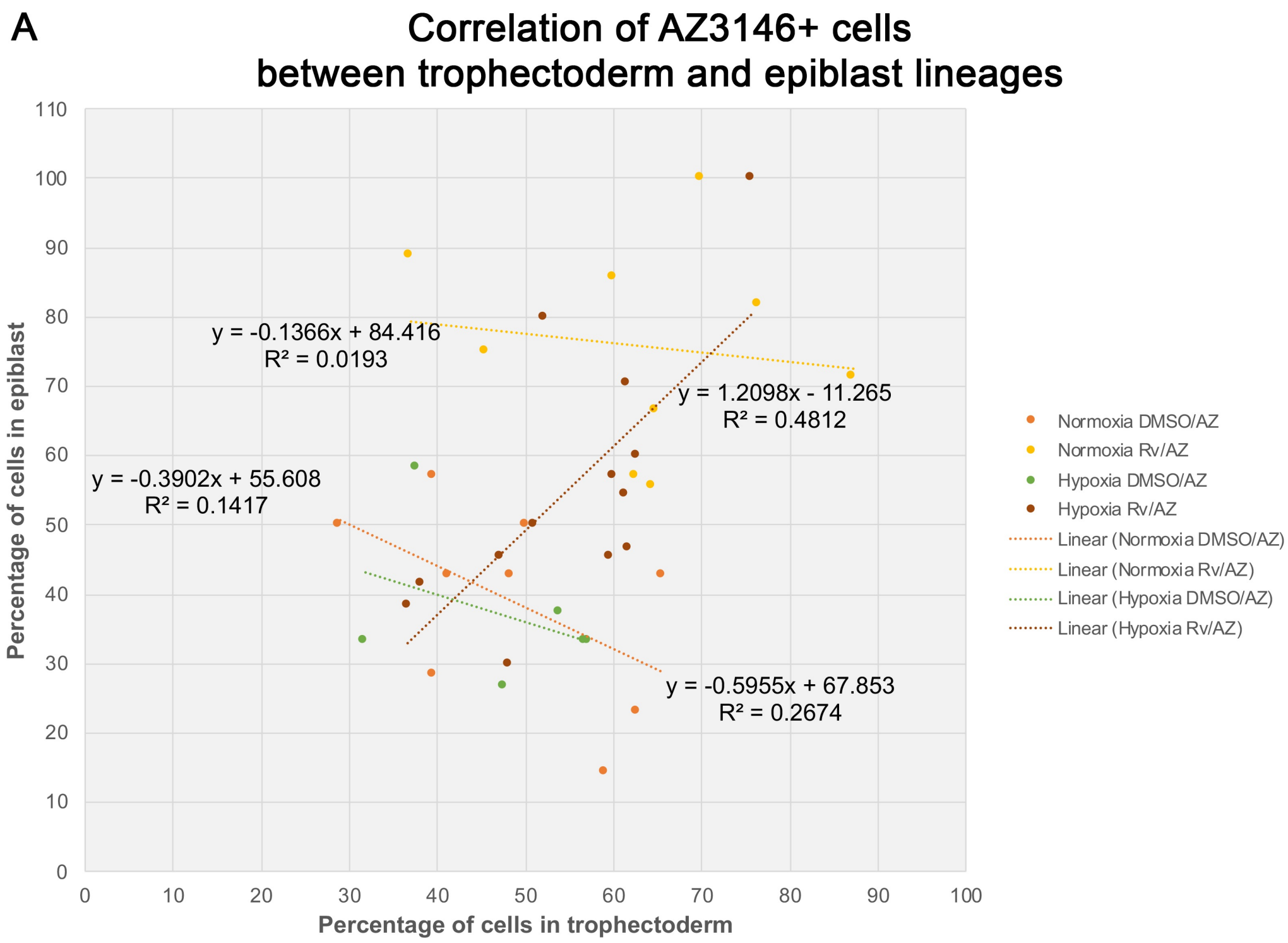
Correlation of AZ3146+ cells
between trophectoderm and epiblast lineages
Percentage of cells in epiblast
Percentage of cells in trophectoderm
0
10
20
30
40
50
60
70
80
90
100
110
y = -0.1366x + 84.416
R² = 0.0193
y = 1.2098x - 11.265
R² = 0.4812
y = -0.3902x + 55.608
R² = 0.1417
y = -0.5955x + 67.853
R² = 0.2674
Normoxia DMSO/AZ
Normoxia Rv/AZ
Hypoxia DMSO/AZ
Hypoxia Rv/AZ
Linear (Normoxia DMSO/AZ)
Linear (Normoxia Rv/AZ)
Linear (Hypoxia DMSO/AZ)
Linear (Hypoxia Rv/AZ)

Figure S. 5

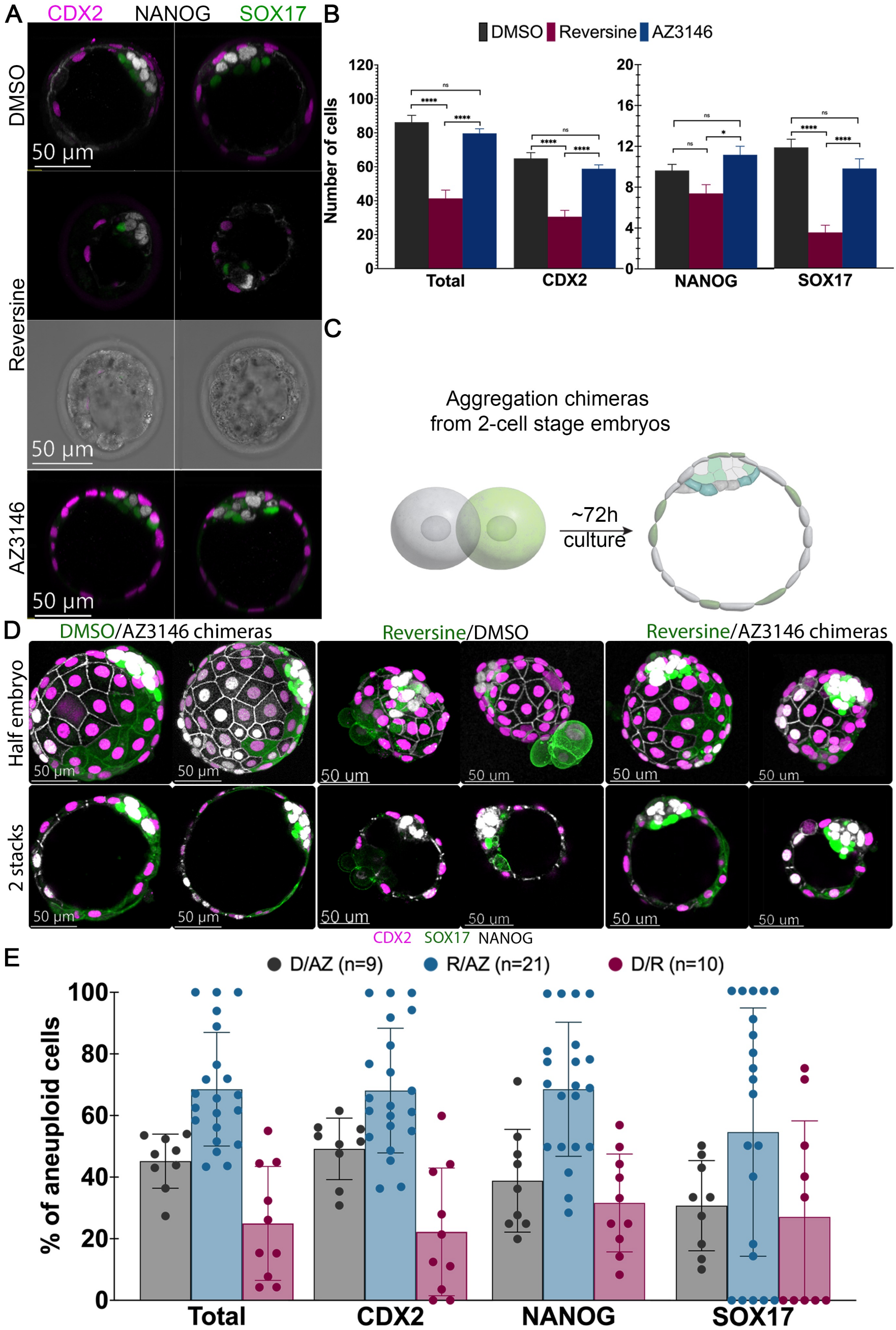
A
CDX2
NANOG
SOX17
DMSO
Reversine
AZ3146
50 µm
B
DMSO
Reversine
AZ3146
Number of cells
Total
CDX2
NANOG
SOX17
C
Aggregation chimeras
from 2-cell stage embryos
~72h
culture
Reversine/DMSO
Reversine/AZ3146 chimeras
D
DMSO/AZ3146 chimeras
Half embryo
2 stacks
50 um
E
CDX2
SOX17
NANOG
D/AZ (n=9)
R/AZ (n=21)
D/R (n=10)
% of aneuploid cells
Total
CDX2
NANOG
SOX17

Figure S. 6

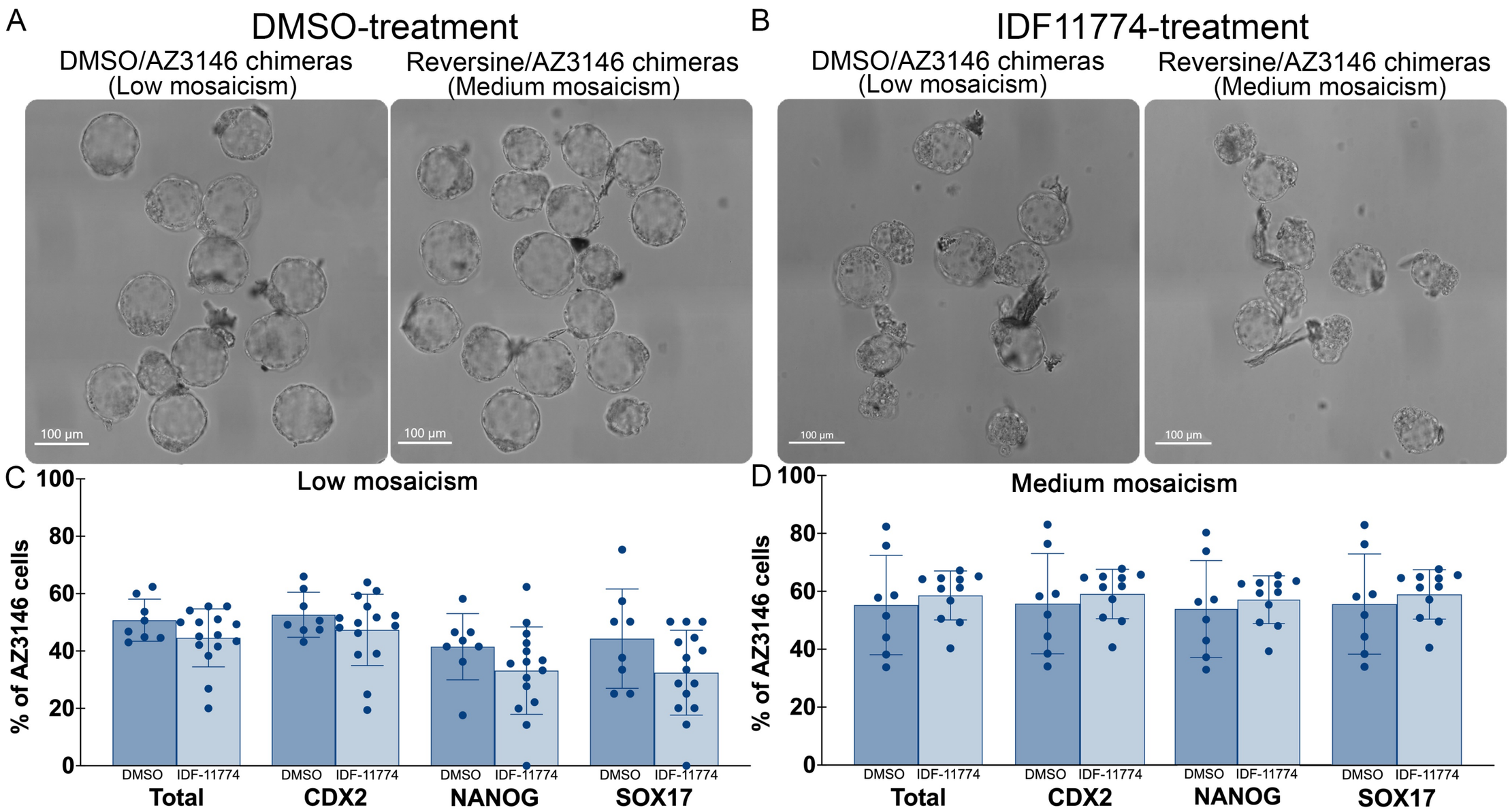
A
DMSO-treatment
DMSO/AZ3146 chimeras
(Low mosaicism)
Reversine/AZ3146 chimeras
(Medium mosaicism)
100 µm
100 µm
B
IDF11774-treatment
DMSO/AZ3146 chimeras
(Low mosaicism)
Reversine/AZ3146 chimeras
(Medium mosaicism)
100 µm
100 µm
C
Low mosaicism
% of AZ3146 cells
100
80
60
40
20
0
DMSO
IDF-11774
Total
CDX2
NANOG
SOX17
D
Medium mosaicism
% of AZ3146 cells
100
80
60
40
20
0
DMSO
IDF-11774
Total
CDX2
NANOG
SOX17